Bioactive Materials 28 (2023) 74–94

Contents lists available at ScienceDirect

Bioactive Materials

journal homepage: www.keaipublishing.com/en/journals/bioactive-materials

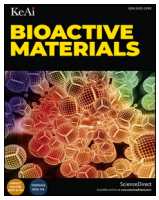

Engineering homologous platelet-rich plasma, platelet-rich plasma-derived exosomes, and mesenchymal stem cell-derived exosomes-based dual-crosslinked hydrogels as bioactive diabetic wound dressings

Bianza Moise Bakadia [a,c], Abeer Ahmed Qaed Ahmed [d], Lallepak Lamboni [a], Zhijun Shi [a], Biampata Mutu Mukole [e], Ruizhu Zheng [a], Mazono Pierre Mbang [c], Bi Zhang [b], Mario Gauthier [f], Guang Yang [a,*]

[a] Department of Biomedical Engineering, College of Life Science and Technology, Huazhong University of Science and Technology, Wuhan, 430074, China
[b] College of Life Science and Technology, Key Laboratory of Molecular Biophysics of MOE, Huazhong University of Science and Technology, Wuhan, China
[c] Institut Supérieur des Techniques Médicales de Lubumbashi, Lubumbashi, Congo
[d] Department of Molecular Medicine, Biochemistry Unit, University of Pavia, 27100, Pavia, Italy
[e] Institut National de Recherche Biomédicale, Ministère de la Santé, Congo
[f] Department of Chemistry, University of Waterloo, Waterloo, Ontario, N2L 3G1, Canada

ARTICLE INFO

Keywords:
Platelet-rich plasma (PRP)
Exosomes (Exos)
Silk protein
Dual-crosslinked hydrogel
Diabetic wound

ABSTRACT

The management of diabetic wounds remains a critical therapeutic challenge. Platelet-rich plasma (PRP) gel, PRP-derived exosomes (PRP-Exos), and mesenchymal stem cell-derived exosomes (MSC-Exos) have demonstrated therapeutic potential in wound treatment. Unfortunately, their poor mechanical properties, the short half-lives of growth factors (GFs), and the burst release of GFs and exosomes have limited their clinical applications. Furthermore, proteases in diabetic wounds degrade GFs, which hampers wound repair. Silk fibroin is an enzyme-immobilization biomaterial that could protect GFs from proteases. Herein, we developed novel dual-crosslinked hydrogels based on silk protein (SP) (sericin and fibroin), including SP@PRP, SP@MSC-Exos, and SP@PRP-Exos, to promote diabetic wound healing synergistically. SP@PRP was prepared from PRP and SP using calcium gluconate/thrombin as agonist, while SP@PRP-Exos and SP@MSC-Exos were derived from exosomes and SP with genipin as crosslinker. SP provided improved mechanical properties and enabled the sustained release of GFs and exosomes, thereby overcoming the limitations of PRP and exosomes in wound healing. The dual-crosslinked hydrogels displayed shear-induced thinning, self-healing, and eradication of microbial biofilms in a bone-mimicking environment. *In vivo*, the dual-crosslinked hydrogels contributed to faster diabetic wound healing than PRP and SP by upregulating GFs expression, down-regulating matrix metalloproteinase-9 expression, and by promoting an anti-NETotic effect, angiogenesis, and re-epithelialization. Hence, these dual-crosslinked hydrogels have the potential to be translated into a new generation of diabetic wound dressings.

1. Introduction

Diabetes mellitus is a chronic disease characterized by high blood glucose levels that, over time, cause substantial harm to the vascular and nervous systems, among others [1]. Its increasing prevalence is a serious issue as it negatively impacts patients' health and is thought to have contributed to 4 million deaths worldwide in 2017 [2]. The prevalence of diabetes mellitus was valued at 9.3% (463 million people) worldwide in 2019, and estimated to increase to 10.2% (578 million people) by 2030, and to 10.9% (700 million) by 2045 [2,3]. Moreover, diabetes can trigger a cascade of complications leading to diabetic ulcers, which affect 25% of diabetic patients [4,5]. Moreover, between 50% and 70% of lower limb amputations in diabetic patients are preceded by diabetic wounds [4]. In fact, it is estimated that every 20 [5] to 30 s [4], one leg is amputated owing to diabetic wounds.

Diabetes delays the wound-healing process by affecting all the

Peer review under responsibility of KeAi Communications Co., Ltd.
* Corresponding author.
E-mail address: yang_sunny@yahoo.com (G. Yang).

https://doi.org/10.1016/j.bioactmat.2023.05.002
Received 28 December 2022; Received in revised form 23 April 2023; Accepted 3 May 2023

typical stages of wound healing [4]. This has a long-term detrimental impact on mortality, morbidity, and quality of life [4]. The lack of growth factors (GFs), reduced microvasculature, NETosis, elevated pro-inflammatory cytokines and proteases, impaired cellular functions, and microbial infection could be considered leading causes of chronic and even non-healing wounds in diabetes patients [4,6]. Therefore, delivering GFs, inducing neovascularization, inhibiting inflammation and oxidative stress, using anti-proteases to protect GFs and the extracellular matrix (ECM), recruiting active cells, and inhibiting bacterial activity constitute therapeutic approaches that can be exploited in diabetic wound management [7]. Traditionally, the clinical management of diabetic wounds consists in graft transplantation, surgical debridement, negative pressure treatment, and regular dressing changes [8]. Unfortunately, these treatments are unsuccessful for many patients due to compromised cellular activity and a deficiency of bioactive factors in the wound microenvironment [4,9]. This limitation to conventional therapy necessitates the development of a novel treatment strategy to accelerate diabetic wound healing [9,10].

In recent years, great emphasis has been placed on using GFs in tissue repair [11]. Platelets are a primary source of GFs with a positive impact on wound healing. Platelet-rich plasma (PRP), the first generation of platelet concentrates [12], is platelet-enriched blood plasma obtained through two-step centrifugation of whole anticoagulant blood [11]. The source of PRP can be autologous, homologous, or heterologous [13,14]. In contrast, the second generation of platelet concentrates [12], platelet-rich fibrin (PRF), which is extracted from coagulant whole blood after one step of centrifugation, is to be strictly autologous [15]. The advantage of PRP lies upon its use both in homologous [14,16] and heterologous [13] applications without adverse effects, as demonstrated in small animals (mouse, rat, etc.); in these cases, the limited blood volume does not allow obtaining a sufficient amount of PRP to cover the prolonged period of chronic healing [13]. Additionally, homologous PRP has been suggested for the treatment of animals with impaired hemodynamic circumstances [14], hematologic disorders, in multidrug therapy [16], or even in cases when the patient's overall health precludes the use of their blood for the preparation of this concentrate [13]. The advantages of using autologous PRP to treat lesions in various tissues and in many species has been evaluated [14,17]. Nevertheless, research on the efficacy of homologous PRP therapy needs further investigation and extension to many species [14]. Herein, the administration of homologous PRP was preceded by a minor crossmatch test to avoid rejection by the immune system.

PRP gel, a clinically approved regenerative medicine consisting in a polymeric fibrin network produced by the combination of PRP and an activator (calcium chloride, thrombin, calcium chloride with thrombin, or collagen type 1), contains a variety of bioactive factors generated by platelet degranulation, such as GFs, cytokines, and chemokines [18]. In addition to these components, the activation of PRP results in the release of extracellular vesicles, such as exosomes [19]. Recently, exosomes have received much attention in regenerative medicine [8,20]. They have the aptitude to transport significant cargo loads of GFs, mRNAs, and micro-RNAs, while protecting their components against degradative chemicals or enzymes. Due to their stability and non-immunogenicity, they are ideal vehicles for nano-delivery therapies [8]. Exosomes control cell-to-cell communication throughout, by transferring their cargo to target cells, thus affecting their functions [19]. Most importantly, exosomes do not differ between species and possess biological properties comparable to their source cells [21]. Consequently, signals can be transferred between species, and exosomes from different species can be collected and prepared for use in the clinic [21]. It was shown in several studies that exosomes from PRP (PRP-Exos) and other cells, such as mesenchymal stem cells (MSC-Exos), can accelerate the healing of chronic cutaneous wounds [8]. MSCs possess substantial potential for tissue regeneration. It was shown that MSCs have the therapeutic ability to regenerate tissues such as bone and skin [22]. MSCs can be extracted efficiently from a range of tissues, but those from bone marrow or adipose tissue are commonly studied and usually used in *in vitro* experiments or clinical studies [23,24]. Bone marrow MSCs (BM-MSCs) have a higher differentiation potential in different lineages than other somatic stem cells and are less immunogenic [25,26]. Recent findings suggest that transplanted stem cell therapy, mainly through secreting extracellular vesicles, may act via a paracrine pathway instead of direct differentiation [27,28]. Therefore, MSC-Exos may be utilized as a substitute for MSC therapy. In this study, we extracted MSC-Exos from BM and PRP-Exos from PRP gel, and used them to treat diabetic wounds.

In clinical and laboratory settings, treating diabetic non-healing wounds with PRP gels and exosomes may promote wound healing significantly [8,23]. Nevertheless, there is at least one report on unsatisfactory response to the management of diabetic wounds in clinics due to the low physical and thermal stability, quick breakdown, and poor mechanical properties of PRP gels [29,30], as well as the rapid clearance rate of GFs [30] and exosomes [31]. Furthermore, an elevated protease concentration in diabetic wound fluids degrades most GFs [30]. More importantly, the limited half-life of GFs during wound healing limits their biological applications in clinics. This causes the PRP gel [32] and exosomes [33] to have poor clinical outcomes, and fails to accelerate diabetic wound healing. Hence, developing a biocompatible and biodegradable dual-crosslinked hydrogel vehicle with good mechanical strength, a lower degradation rate [34], and self-healing ability to continuously release and preserve the biological functions of encapsulated bioactive factors is critical for exosome- and PRP-based treatments in diabetic wound healing. Thus, we aimed at combining PRP or exosomes with a polymer displaying protease inhibitory capability as a clinical strategy to enhance their respective therapeutic effects.

Silk protein (SP), composed of sericin (15–35%) and fibroin (65–85%), is a naturally occurring protein from the silkworm utilized for the manufacture of biomaterials, and is a Food and Drug Administration (FDA)-approved protein suitable to work in conjunction with PRP and exosomes [35]. Silk sericin (SS) is widely used in tissue repair due to its excellent biocompatibility, antioxidant, anti-inflammation, mitogenic, anticoagulation, moisturizing, and anti-wrinkle properties, which may accelerate wound healing [36,37]. Silk fibroin (SF) likewise has excellent properties such as high strength and flexibility, blood compatibility, biocompatibility, oxygen permeability, and water permeability, so it can be used in tissue engineering applications [38]. In addition, SF is an enzyme-immobilization material that can protect GFs from enzymatic hydrolysis and prolong biological activity in diabetic wounds [39]. SF is known to stimulate the NF-kB signaling pathway, which further results in a rise in the expression of different GFs [40]. SP has been developed into commercial materials such as U.S. FDA-cleared SERI® surgical scaffolds (Allergan Medical; out of production since the end of 2021), Sofsilk™ Silk Sutures (Medtronic), DermaSilk (Alpretec), Epifibroin (Medisilk Spa), and Silk Voice® (Sofrogen) [41,42]. Furthermore, the Sidaiyi® wound dressing is a China Food and Drug Administration (CFDA)-approved product for burns, as well as partial and full-thickness wound management [43]. More clinical trials using SP composite wound dressings are ongoing for various medical applications (NCT01539980, NCT02643680) [41,42]. In this study, to develop an SP@PRP dual-crosslinked hydrogel system through a one-step reaction, a mixture of calcium gluconate and thrombin was used as gelation mediator for solution blends of SP and PRP. In this system, thrombin in the presence of Ca^{+2} promotes the conversion of fibrinogen into fibrin. Subsequently, fibrin forms a mechanically and chemically stable network of fibrin monomers, strengthened through covalent crosslinking by factor XIIIa; this transglutaminase catalyzes the crosslinking of glutamine and lysine residues (Scheme 1B) [44]. Since SP also contains glutamine and lysine [45–48], this transglutaminase can likewise crosslink the SP and PRP components through their glutamine and lysine residues. Moreover, Ca^{+2} can interact with the amino groups of SP, forming electrostatic bonds (Scheme 1C) further strengthening the hydrogel network, in addition to H-bonding [49]. Consequently, the dual-crosslinked hydrogel SP@PRP results from both covalent and

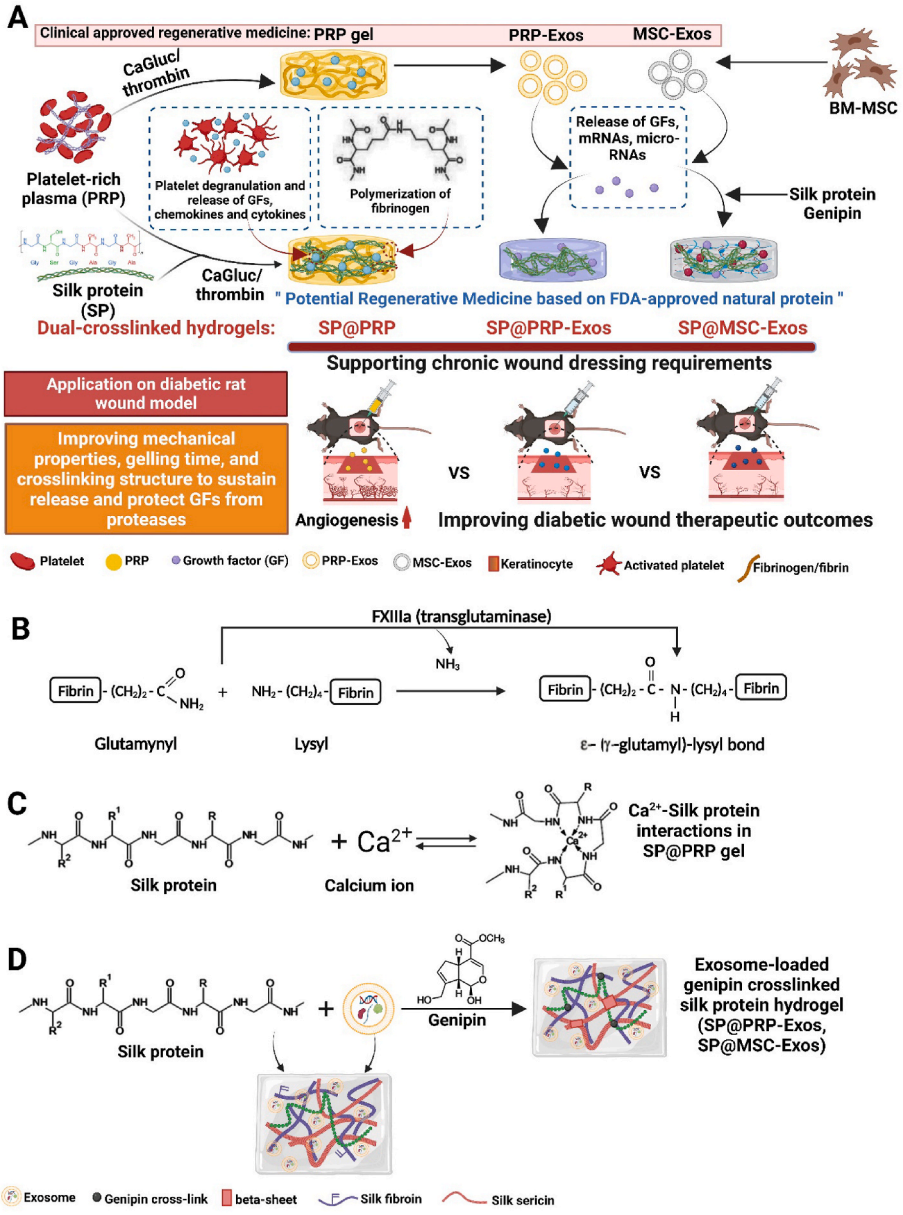

Scheme 1. Schematic illustration of (A) the synthetic process for dual-crosslinked hydrogels (SP@PRP, SP@PRP, and SP@PRP) and their use as diabetic wound dressings; (B) Factor XIIIa catalyzes a chemical reaction resulting in insoluble fibrin highly covalently crosslinked through glutamine and lysine residues; (C) Ca^{+2}-silk protein interactions in SP@PRP activated with calcium gluconate, and (D) formation of exosome-loaded genipin-crosslinked silk protein hydrogels.

non-covalent crosslinking. For the fabrication of SP@PRP-Exos and SP@MSC-Exos, genipin (GNP) was used as chemical crosslinker in solutions of SP and exosome blends. In these SP-based hydrogels, the chemical crosslinker (GNP) controls the formation of β-sheet physical crosslinks in addition to creating covalent bonds, resulting in a dual-crosslinked hydrogel based upon chemical and physical crosslinks, with marked increased hydrogel strength due to β-sheet structures (Scheme 1D) [50].

In this study, we hypothesized that dual-crosslinked hydrogels based on SP, incorporating either PRP, PRP-Exos, or MSC-Exos, could improve diabetic wound healing as compared with PRP gel and SP gel. To confirm this, the dual-crosslinked hydrogels were characterized morphologically, mechanically, physiochemically, and biologically. Furthermore, a full-thickness diabetic wound model in rats was established, and SP@PRP gel, SP@PRP-Exos, and SP@MSC-Exos, delivering PRP, PRP-Exos, and MSC-Exos, respectively, were administered to repair rat skin defects in the diabetic model. Thus, we developed a new therapy based on dual-crosslinked hydrogels offering mechanical support and self-healing properties, while protecting and releasing GFs and exosomes sustainably, providing anti-NETosis and antimicrobial activities, and enhancing diabetic wound healing.

2. Materials and methods

2.1. Cardiac puncture

Blood sampling, approved by the Ethics Committee of the Hubei Provincial Center for Disease Control and Prevention (approval no. 202120167), was performed through cardiac puncture to collect higher blood volumes, which were transferred to EDTA-centrifuge tubes to extract PRP and PRP-Exos. Thirty-two healthy non-diabetic rats (body mass 200–250 g) were deeply anaesthetized by an intraperitoneal injection of 10% chloral hydrate (350 mg/kg). These rats were positioned in dorsal recumbency. Blood was drawn from the ventricular region (left

or right) to prevent the heart from collapsing. The index finger was then put close to the lower left rib, where the strongest palpitation was felt, without exerting pressure. The heart was situated roughly between the fourth and sixth ribs. As illustrated in Fig. S1 and Scheme 2, a 20-gauge needle with a syringe was inserted between two ribs at an angle of 30–45°. The plunger was gently pushed to generate a vacuum within the syringe and kept in the same position until a blood drop entered the needle. The plunger was gradually pulled to draw the needed blood volume without moving the needle. Then, the blood was withdrawn slowly to prevent the heart from collapsing. The rats were euthanized immediately following blood sampling.

2.2. PRP extraction and activation

The rats' whole blood, withdrawn through cardiac puncture and placed in EDTA-centrifuge tubes, was then gently agitated to blend it thoroughly with the anticoagulants. The blood was centrifuged twice to separate platelets from red blood cells (RBCs) and leukocytes using a high-speed centrifuge (Hunan Xiangli Scientific Instruments Co., Ltd., China). In summary, the blood was centrifuged for several minutes at a low g force (900 g for 5 min), yielding four constituent fractions, including plasma, platelets, leucocytes, and RBCs. The two top layers (plasma and platelets) were transferred to a fresh tube and centrifuged at 1500 g for another 15 min. Prostaglandin E1 (100 ng/mL) was added to the plasma to preclude platelet activation during PRP isolation. The precipitated platelets were resuspended in the remaining plasma to generate PRP after discarding most (three-quarters) of the supernatant plasma layer. Each PRP was divided into three aliquots of 1.8 mL and activated with CaGluc (0.2 mL, 10%), thrombin (0.2 mL, 10%), or a solution containing a mixture of CaGluc (0.1 mL, 5%) and thrombin (0.1 mL, 5%), respectively. All the PRP samples were incubated for 20 min at 37 °C in a water bath to generate PRP gels (Scheme 2A).

2.3. Extraction of PRP-derived exosomes

Gradient ultracentrifugation and ultrafiltration techniques were used to extract and purify exosomes (Scheme 2B) [51]. Several agonists (CaGluc, thrombin or their mixture) were utilized to stimulate the release of exosomes from PRP. The samples (the above-mentioned PRP gels) were handled in 15 mL sterile 70 Ti polycarbonate bottles. Centrifugation was performed at 4 °C, using an ultracentrifuge (Optima L-80XP, Beckman, USA). The activated PRP was centrifuged successively at 300 g for 10 min, 1500 g for 15 min, and 3200 g for 20 min to eliminate cellular debris. The exosomes were then separated from membrane vesicles by centrifugation at 20,000 g for 30 min at 4 °C. The pellet was eliminated after each centrifugation and the supernatant was utilized in the subsequent step. The supernatant from the last centrifugation was filtrated through a 0.22 μm filter. The exosomes were obtained by ultracentrifugation of the filtrate at 100,000 g for 70 min at 4 °C, washed in sterile PBS, and then pelleted under the same conditions. The pellets were reconstituted with 500 μL of sterile PBS and centrifuged using a Nanosep centrifugal device, 100K at 14,000 g and 4 °C for 20 min. The filtrate was carefully reconstituted in 200 μL of sterile PBS comprising phosphatase and protease inhibitor cocktails (Shaanxi Zhonghui Hecai Biomedical Technology Co., Ltd., China) and stored at −80 °C until further use.

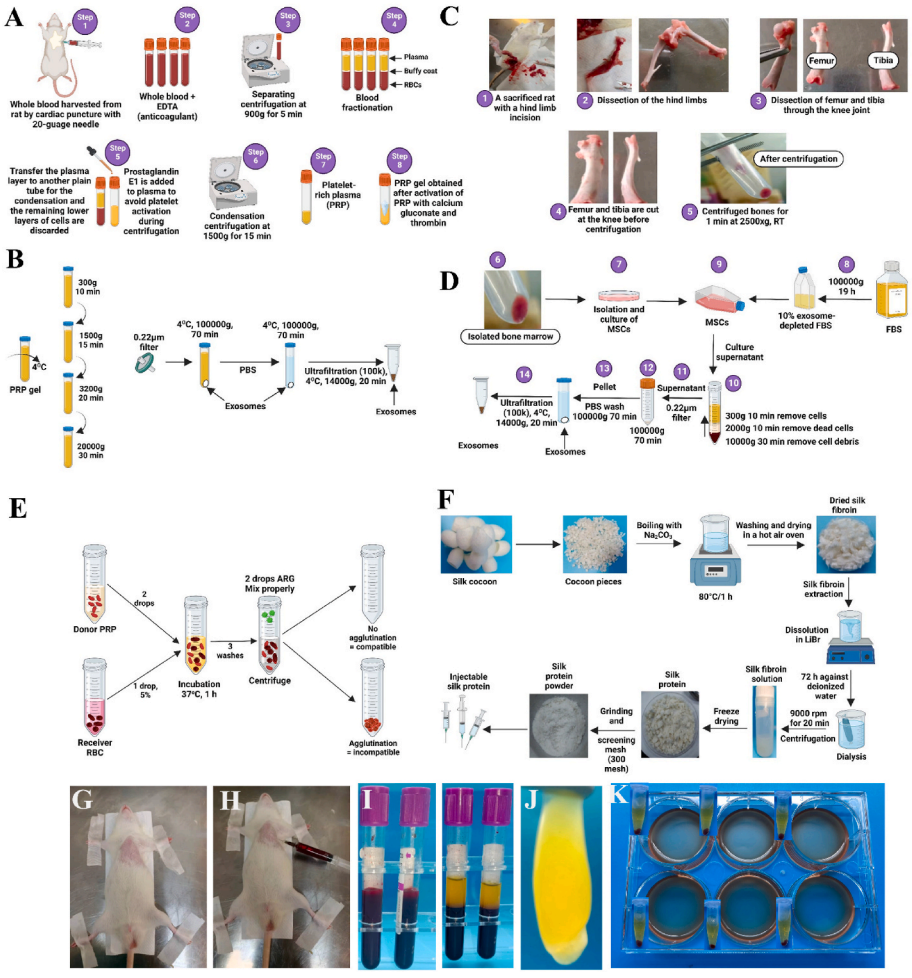

Scheme 2. PRP gel preparation, exosome extraction, silk fibroin extraction, and results of blood minor crossmatch. Schematic illustration of (A) PRP extraction and PRP gel preparation, (B) PRP exosomes isolation by gradient ultracentrifugation and ultrafiltration, (C) long bone dissection and isolation of bone marrow, (D) BM-MSCs and MSC-derived exosomes isolation by gradient ultracentrifugation and ultrafiltration, (E) blood minor crossmatch, and (F) preparation of injectable silk fibroin, (G–H) rat blood sampling by cardiac puncture, (I) blood fractionation by centrifugation in EDTA tubes, (J) platelet aggregation in plasma without prostaglandin E1 after the second centrifugation step, (K) representative images for blood minor crossmatch. The absence of clumping in the six-well plate and hemolysis in tubes indicated that the donor's PRP was compatible with the recipient's.

2.4. Isolation of MSC-derived exosomes

Rat bone marrow-derived MSCs were isolated from rats as described in Scheme 2C. These MSCs were cultured in Dulbecco's Modified Eagle Medium (DMEM) supplemented with 10% Fetal Bovine Serum (FBS). At nearly 90% confluency, cells were rinsed 3 times with PBS, and the medium was changed with 5 mL of DMEM enriched with exosome-depleted FBS (Scheme 2D). After 48 h of incubation, the cultured medium was collected and cleared using continuous centrifugation at increasing speeds. The pellet was discarded at each centrifugation phase, and the supernatant was used for the following process. The exosomes were subsequently pelleted by ultracentrifugation of the final supernatant at 100,000 g. The pellet was rinsed with PBS to eliminate contaminating proteins before being centrifuged at 100,000 g. The pellets were reconstituted in 500 μL of sterile PBS and then centrifuged using a Nanosep centrifugal device at 100 KD at 14,000 g at 4 °C for 20 min. The filtrate was carefully reconstituted in 200 μL of sterile PBS containing phosphatase and protease inhibitor cocktails and stored at −80 °C until further use.

2.5. Identification of exosomes

First, the exosome size and concentration distribution were precisely assessed using Particle Metrix ZetaView® nanoparticle tracking analysis (NTA) and high-sensitivity flow cytometry for nanoparticle analysis (NanoFCM Inc., China). Further, the morphology of the exosomes was examined using a transmission electron microscope (TEM, HITACHI, HT7700, Japan). The exosomes were deposited onto a 2 nm copper grid and stained negatively with 3% phosphotungstic acid for 2 min. The particle size statistics of TEM images also served to determine the exosome size. Finally, western blotting (WB) was carried out as follows: Proteins were extracted from the cells or exosomes with RIPA lysis buffer, and the protein concentration was measured with a Lowry protein assay kit. The lysates were diluted at a volume ratio of 1:3 with protein loading buffer (4 ×) and heated to 95 °C for 10 min. The protein extracts were separated on 12% sodium dodecyl sulphate polyacrylamide electrophoresis gel (SDS-PAGE) at 110 V for 1 h and blotted onto a nitrocellulose membrane for 90 min at 270 mA. The membranes were then blocked for 2 h with 5% (w/v) bovine serum albumin (BSA) in TBST (Tris-buffered saline, H_2O, 0.1% Tween-20). Afterwards, the membranes were incubated with primary antibodies (anti-CD9; 1:500 dilution; Proteintech), (anti-CD63; 1:500 dilution; Santa Cruz Biotechnology), and (anti-CD81; 1:1000 dilution; Proteintech) at 4 °C overnight, followed by washing in TBST and incubation with secondary antibodies at RT for 2 h. The TBST was used to remove the excess secondary antibody, and the immunoreactive bands were visualized with a two-colored infrared laser system odyssey CLx (Li-COR, Inc., USA).

2.6. Preparation and composition of hydrogels

SS and SF solutions were prepared by dissolving them in PRP with vigorous stirring at 37 °C for 1 h. The preparations were then mixed with CaGluc and thrombin (Table 1). After 20 min of incubation at 37 °C, the final dual-crosslinked hydrogels were identified as S10F90@PRP, S20F80@PRP, S30F70@PRP, and S40F60@PRP (Table 1). Furthermore, a SP (S30F70) solution (2%) was prepared by heating to 90 °C for 20 min and cooling to room temperature (RT). It was then mixed with PRP-Exos or MSC-Exos (2%) at 4 °C, and crosslinked with GNP (0.1%) for 30 min to form SP@PRP-Exos and SP@MSC-Exos dual-crosslinked hydrogels, respectively. SP (S30F70) gel was used as a control at 4% concentration without a chemical crosslinker (GNP).

2.7. Determination of growth factors in PRP and SP@PRP gels

The concentration of GFs was estimated using an ELISA kit at relevant time intervals. The gels (1 g) prepared in 24-well plates were immersed in 5 mL of fresh DMEM, and incubated at 37 °C with 5% CO_2 for 30 min to 7 days to enable the release of GFs. Samples (5 mL) of DMEM were withdrawn from the specimens after 30 min, 1 h, 4 h, 1 day, 2 days, 3 days, 4 days, 5 days, 6 days, and 7 days, stored at −80 °C for future use, and replaced with 5 mL of fresh DMEM. The manufacturer's instructions for the ELISA kit (Proteintech, Rosemont, IL 60018, USA) were followed for the analysis. The concentration of GFs at each time point was evaluated to determine the optimal time for GF release. This test was carried out twice for improved accuracy.

2.8. Antimicrobial studies of the hydrogels

2.8.1. Antimicrobial evaluation using the disk and agar well diffusion methods

The disk diffusion method was used to measure the antibacterial activity of PRP gel, SP@PRP gel, SP@PRP-Exos, and SP@MSC-Exos prepared in 24 well-plates, while the agar well diffusion method was used for PRP (200 μL) as previously described [36]. The microbes used for this test included *Methicillin-resistant* Staphylococcus aureus (MRSA), Staphylococcus aureus *(S. aureus)*, Escherichia coli *(*E. coli*)*, and Pseudomonas aeruginosa *(*P. aeruginosa*)* cultured on their specific media. *S. aureus* and MRSA were cultured on mannitol salt agar (MSA), while *P. aeruginosa* and *E. coli* were cultured on MacConkey (MAC). *All the bacteria were tested for antimicrobial susceptibility using Muller Hinton Agar (MHA) and their specific medium*. Continuous dilutions were used to test the bacterial concentrations. Agar plates were then inoculated with 10^7 CFU/mL of the corresponding bacteria, and gels (1 cm diameter) were placed onto the agar before incubation at 37 °C for 24 h. Then the diameter of inhibitory activity was evaluated using a ruler. All the tests were carried out in triplicate.

2.8.2. Antimicrobial activity against microbial biofilms in an environment mimicking bone conditions in the absence of immunity

2.8.2.1. Preparation of hydroxyapatite discs. Hydroxyapatite (HA) discs were utilized as microbial biofilm growth surfaces. HA powder was compressed under uniaxial pressure of 5 MPa into discs with a diameter of 10 ± 0.03 mm and a thickness of 1 ± 0.04 mm. The HA discs were then sintered at 900 °C for 3 h. The surface morphology of the HA discs was analyzed using field emission scanning electron microscopy (FESEM, Nova33NanoSEM450, FEI, USA).

2.8.2.2. Scanning electron microscopy analysis of bacterial biofilms on hydroxyapatite discs. Different bacterial dilutions were incubated on HA discs for 48 h at 37 °C to allow biofilm formation, and the biofilm-covered HA discs were treated with different gels for 24 h. The HA

Table 1
Composition of SP@PRP gels.

Ingredient/ Formulation	PRP	S10F90@PRP	S20F80@PRP	S30F70@PRP	S40F60@PRP
Sericin (mg)	0	10	20	30	40
Fibroin (mg)	0	90	80	70	60
PRP (mL)	1.8	1.8	1.8	1.8	1.8
CaGluc/Thrombin (mL)	0.2	0.2	0.2	0.2	0.2

discs covered with biofilm, treated and untreated, were observed by FESEM as described previously [36].

2.9. Wound healing inserts (culture-inserts) to detect cell migration

The migratory ability of NIH-3T3 cells was assessed using a *2 well* silicone *insert* with 0.5 mm cell free gap (culture-insert 2 well in μ-dish 35 mm). In brief, the cell suspension was seeded in culture inserts (3.5×10^4 cells/chamber) and incubated at 37 °C. After cell attachment for 24 h, the cells were serum-starved for 12 h. Tweezers were used to remove the silicone culture inserts and create a 0.5 mm wound gap. After PBS washes, the cells were incubated with gels at a concentration of 25 μg/mL. Cell migration was visualized at 0, 24, and 48 h with a light microscope and computed using the ImageJ software, to calculate the percentage migration (n = 3). The migration rate (MR) was evaluated using equation (1),

$$\mathrm{MR}\ (\%) = \frac{R0 - \mathrm{Rn}}{R0} \quad (1)$$

where R0 is the original wound area, and Rn is the residual wound area.

2.10. Blood minor crossmatch

The blood minor crossmatch tests the donor PRP with the concentrated erythrocytes of the receiver, using the same techniques as the search for irregular antibodies (Scheme 2E) [52,53]. This test determines whether the donor's PRP is compatible with the recipient [53]. The rat's donor PRP was mixed with the diabetic recipient rat's RBCs and stored at 37 °C for 1 h before mixing with rabbit anti-rat IgG (1:20 dilution; Invitrogen). The absence of clumping indicated that the donor PRP was appropriate for the recipient. If the PRP from the donor clumped, it could not be used for the recipient and could cause serious health problems.

2.11. Animal models

The animal studies were approved by the Ethics Committee of the Hubei Provincial Center for Disease Control and Prevention (approval no. 202120167). Thirty-eight healthy male adult Sprague Dawley (SD) rats, constituting the 5 main comparative animal treatment groups, and 6 SD rats constituting the diabetic control group, weighing between 200 and 250 g (7–8 weeks old), were acclimatized for 7 days in standard cages at the Hubei Provincial Center for Disease Control and Prevention's animal house for the duration of this study. Throughout the experiment, the animals were maintained under standardized conditions, including a constant temperature of 24 ± 2 °C, a relative room humidity level of 50–70%, and an alternating 12 h day and 12 h night cycle. They also had unlimited access to a high-fat diet and water.

2.11.1. Induction of diabetes

After fasting for nearly 16 h with only water available ad libitum, 44 rats, including 38 in the treatment groups and 6 in the diabetic control group, received a single intraperitoneal injection of streptozotocin (STZ) (50 mg/kg) each to initiate the severe diabetes mellitus experimental model. A 0.2 mL drop of blood was drawn with a syringe from the tail vein of each rat three days after induction, and the blood was tested using a Sinocare Glucometer Blood Glucose Meter Kit. The diabetic rats in this study had glycemia greater than 14 mmol/L or >250 mg/dL on day 21 after STZ injection.

2.11.2. Induction of wounds

All the rats were anaesthetized intraperitoneally with 3% sodium pentobarbital (0.26–0.3 mL/100 g) after being diagnosed with severe diabetes. The dorsal hair of the rats was removed with a clipper and cleaned with 70% ethanol before wounding. A biopsy punch with 10 mm diameter was used to generate a standard full-thickness wound.

2.11.3. Treatment of wounds

Various gel-based treatments were applied topically to the rats after a minor crossmatch test every two days for 14 days. There were 5 main comparative animal treatment groups of 7 rats each (3 rats died during the induction of diabetes), forming group 1 (SP treatment), group 2 (PRP gel treatment), group 3 (SP@PRP gel treatment), group 4 (SP@PRP-Exos gel treatment), and group 5 (SP@MSC-Exos gel treatment). The rats in groups 2–5 were subjected to new wounds, and their treatment was inverted on the 14th postoperative day (POD): The rats in group 2 were treated with SP@PRP gel, the rats in group 3 with PRP gel, the rats in group 4 with SP@MSCs-Exos gel, and the rats in group 5 with SP@PRP-Exos gel. The control group of 6 diabetic rats with untreated wounds was also included for further evaluation.

2.11.4. Gross evaluation of wound contraction

Wound area reduction over time has been shown to illustrate the healing process in diabetic wounds. The wound areas on days 7 and 14, in particular, significantly predict wound healing [22]. The wounds were examined macroscopically on days 0, 3, 7, 10, and 14 and wound closure was estimated by photographing with a digital camera. The percentage of wound contraction was assessed with ImageJ (NIH, USA) to compute the wound healing rate (WHR) using equation (2),

$$\mathrm{WHR} = \frac{Ai - \mathrm{Af}}{Ai} \quad (2)$$

where Ai and Af denote the wound area on day 0 and day n, respectively.

2.12. Quantitative reverse transcription polymerase chain reaction (qRT-PCR)

The detailed procedure for ARN extraction and **qRT-PCR is described in the Supplementary material. The** primer sequences used are provided in Table 2.

The materials and methods, including (i) platelet and leukocyte counting; (ii) isolation, culture, and identification of mesenchymal stem cells from rat bone marrow; (iii) particle size statistics for the TEM images, (iv) silk sericin and silk fibroin preparation, (v) physicochemical characterization; (vi) biodegradability evaluation, (vii) rheological properties tests; (viii) release of total protein from SP@PRP-Exos and SP@MSC-Exos gels, (ix) swelling ratio (SR), (x) *in vitro* cell viability and proliferation, (xi) **macrophage treatment with gels under inflammatory conditions, and** (xii) histopathological and immunological analyses are provided in the **Supplementary file.**

Table 2
Primer sequences used for qPCR gene expression analysis.

Target genes	Forward primers (5′ to 3′)	Reverse primers (5′ to 3′)	Genbank ID
IGF-1	ATCTCTTCTAC CTGG CACTCTG	GAAGCAACACTCAT CCACAAT	AH002176.2
VEGF	GCACCCACG AC AGAAGG	TGAACGCTC CA GGATTTA	AY033504.1
TGF-β1	CTGAACCAAGG AGACG GAATAC	GTTTGGGACT GATCC CATTGA	NM_021578.2
EGF	ACCAACACGGA GGGA GGCTACAA	GCGGTCCACGGA TTCAACATACA	NM_012842.1
MMP-9	ATCTCTTCTAGAGACT AGGAAGGAG	CAAGCTGATT GGTT CGAGTAGC	NM_031055

IGF-1, insulin-like growth factor-1; VEGF, vascular endothelial growth factor; TGF-β1, transforming growth factor-β1; EGF, endothelial growth factor; MMP-9, matrix metalloproteinase-9.

2.13. Statistical analysis

All the experiments were carried out in triplicate, and independently repeated at least twice for each assay. The data were statistically analyzed using one-way analysis of variance (ANOVA) followed by Tukey's Multiple Comparison Test in Origin Pro 2018 9.5 (Origin Lab, Berkeley, CA, USA). All the quantitative results are represented as mean ± standard deviation, and differences were considered significant at $P < 0.05$, with * indicating $P < 0.05$, ** indicating $P < 0.01$, *** indicating $P < 0.001$, and NS for no significance.

3. Results

3.1. Preparation and morphology of hydrogels

As shown in Schemes 1 and 2, the PRP was prepared by sampling the blood of rats obtained by cardiac puncture and then gently centrifuging the blood in two steps. As per its definition, for the 32 rats that were included in the study, the platelet concentration in the PRP, $(3.8 \pm 0.4) \times 10^6$ platelets/μL, was 4.4 times higher than that from the initial anticoagulated whole blood, $(8.5 \pm 0.90) \times 10^5$ platelets/μL. In fact, the conceptual PRP model suggests a minimal platelet count of 1×10^6 per microliter [54]. This represents a 3–5 fold increase over the standard concentration of platelets, which ranges from 140,000 to 400,000 platelets/μL in healthy humans [54], as compared with 702,000 to 998, 000/μL in healthy rats [55]. The leucocytes were significantly reduced from $(11 \pm 1) \times 10^3$/μL in whole blood to 9 ± 3/μL in PRP, resulting in leukocyte-poor PRP (LP-PRP) [56], enormously minimizing the risks of immune rejection due to leukocyte antigens. Besides, the inclusion of large numbers of leukocytes in PRP, such as in leukocyte-rich PRP (LR-PRP), leads to a significant increase in pro-inflammatory cytokines delaying wound healing [57]. Therefore, LP-PRP is the best choice for proper tissue regeneration.

To avoid platelet activation during PRP isolation, prostaglandin E1 (PGE1) (100 ng/mL) was added to the plasma before the second centrifugation step, which required a high speed. By comparison, plasma without PGE1 generated weak platelet activation during centrifugation (Scheme 2J), demonstrating the effects of PGE1 in enhancing the preparation effectiveness of PRP and preserving the therapeutic efficiency of the platelets. PGE1 is recognized as a reversible inhibitor of platelet aggregation caused by collagen and adenosine diphosphate, while also increasing cyclic adenosine monophosphate levels within the platelets [58,59]. There is currently no research available on the impact of PGE1 on the preparation of PRP in rats, despite early studies showing that adding PGE1 to human PRP enhanced platelet separation, concentration, and resuspension [58].

Afterwards, PRP was activated with CaGluc, thrombin, or a mixture with equal volumes of CaGluc and thrombin to generate PRP gel (Scheme 2A and S2). We discovered that PRP gel stimulated with CaGluc and thrombin induced the highest concentration (4.5 ± 0.2 μg/μL) of total exosome proteins as compared to CaGluc (4.0 ± 0.2 μg/μL) or thrombin (3.7 ± 0.2 μg/μL) alone, using the Lowry protein assay (Fig. S2). The CaGluc and thrombin mixture induces PRF, producing a soft gel [60]. Platelets within the soft gel can degranulate and release GFs to accelerate wound healing [60]. Some tissues profit from accelerated platelet release or the initiation of a compact fibrin network, such as surgical opening wounds, whereas others take advantage of slow and progressive GFs secretion [60]. The latter was achieved by combining PRP with SP. The fabrication method for SP@PRP dual-crosslinked hydrogels using only CaGluc and thrombin as one-step activation reactions is depicted in Scheme 1. The SP formulation was initially examined by comparing the shear thinning behavior of SP@PRP dual-crosslinked hydrogels with various SS/SF ratios, including S10F90@PRP, S20F80@PRP, S20F80@PRP, and S40F60@PRP (Fig. S3). The preparation procedure for SP@PRP dual-crosslinked hydrogels was essentially similar to that for the PRP gels. To obtain a homogeneous solution, PRP was first mixed with SP containing different SS/SF ratios, and the blend was vigorously stirred at 37 °C for 1 h to dissolve the SP. Following that, a CaGluc and thrombin mixture was added to the solution as gelation facilitator for both materials. Within the SP@PRP dual-crosslinked hydrogels, fibrin networks might form by the previously reported PRP activation process (Scheme 1A, B), while Ca^{2+} ions also can interact with SP via its amine groups (Scheme 1C). As a result, the S30F70@PRP dual-crosslinked hydrogel, with a composition similar to natural SP in terms of SS and SF proportions, exhibited superb shear thinning and a suitable storage modulus (Fig. S4). Therefore, the S30F70@PRP dual-crosslinked hydrogel was employed for subsequent characterization.

In addition to the PRP gels and SP@PRP dual-crosslinked hydrogels, the activation of PRP results in the release of exosomes. Therefore, SP@PRP-Exos dual-crosslinked hydrogels were also prepared. For comparison, the exosomes were extracted from BM-MSC to prepare SP@MSC-Exos dual-crosslinked hydrogels. These BM-MSCs presented a typically spindle-shaped morphology (Fig. 1A–B and S5). Further, MSCs were characterized by immunofluorescent cytochemical staining for the presence of specific markers, including positive MSC markers such as CD105, CD90, and CD73, and CD45 as negative MSC marker. The staining experiments provided confirmation for the morphology and characteristics of MSC (Fig. 1A).

The exosomes were isolated from activated PRP and BM-MSC through low-speed centrifugation, ultracentrifugation, and ultrafiltration (Scheme 2A-D) and characterized by TEM and WB. Additionally, to further establish the size and concentration of MSC-Exos and PRP-Exos, an NTA and nano-flow assay were performed for MSC-Exos and PRP-Exos, respectively. TEM showed that PRP-Exos and MSC-Exos exhibited a round morphology, appearing as a classic cup-shaped vesicle. The majority of PRP-Exos and MSC-Exos had sizes of 60 ± 10 nm (Fig. 3E–F) and 70 ± 20 nm (Fig. 3G–H), respectively, which confirmed the presence of exosomes, in agreement with earlier reports [20]. However, the exosomes from PRP and MSC differed in size: The size of MSC-Exos was noticeably larger than PRP-Exos (Fig. 3E–H and S6) [61]. WB indicated that both types exhibited exosomal surface markers such as CD81, CD63, and CD9, confirming their exosome nature (Fig. 3K and S7).

To prepare the dual-crosslinked hydrogels based on exosomes, SP (S30F70) solution (2%) was mixed with exosomes (2%) and crosslinked with GNP (0.1%). The GNP improves the physical and chemical properties of the hydrogels, resulting in a dual-crosslinked network (Scheme 1D) [50]. Moreover, GNP binds to the amine groups of SP, serving as a molecular bridge connecting polymeric chains and improving the overall stability of the hydrogel network [62]. Blue pigments are formed in the crosslinking process between GNP and SP (Fig. S1 D).

The morphology of the gels was investigated by FESEM imaging (Fig. 2A–D and S8), and the incorporation of exosomes into SP was also confirmed by TEM (Fig. S9). The PRP gels displayed a fibrin network comprising variously sized fibrils crosslinked by fibrinogen. The fibrils were linked together as filaments forming an interconnected porous structure. This should facilitate the transport of nutrients and gas exchange, significantly enhancing cell proliferation [63]. The incorporation of SP into the PRP gels changed the morphology of the fibrils significantly, increasing their size (Fig. S10) and confirming the glue-like property of SS, which facilitates cell adhesion [63]. Additionally, there was a noticeable variation in the network structure of the samples, particularly in terms of pore size and porosity, higher for the SP@PRP dual-crosslinking hydrogel than for the PRP gel (Fig. 2L-M). The SP@PRP-Exos and SP@MSC-Exos dual-crosslinking hydrogels displayed structures with comparable porosity levels but different pore configurations, with the exosomes noticeable in FESEM (Fig. S8) and TEM images (Fig. S9). With the exception of the PRP gel, all the dual-crosslinked hydrogels (SP@PRP gel, SP@PRP-Exos, and SP@MSC-Exos) meet the requirements for skin tissue regeneration in terms of porosity and pore size (ideal pore size range of 20–125 μm, preferred porosity range of 60–90%) [63]. Additionally, they exhibit a

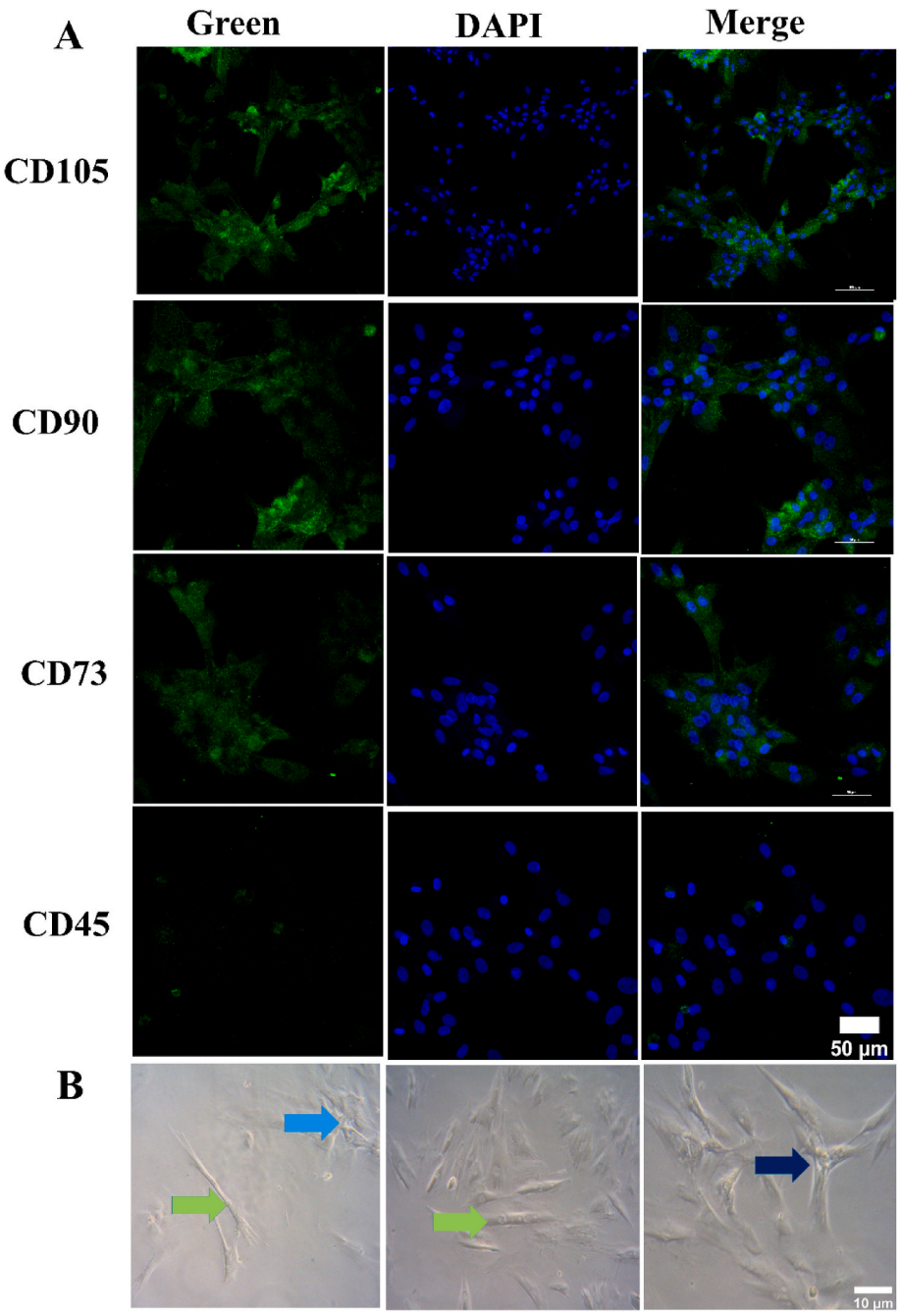

Fig. 1. Characterization of BM-MSCs. (A) Immunofluorescence staining using MSC-positive markers, including CD105, CD90 and CD73, and CD45 as negative marker. The cytoplasm is stained green, while the nuclei are blue. B) MSCS optical microscopic images. BM-MSC morphology with typical spindle shape (light green arrow), colony formed during cell culture (light blue arrow), morphology of MSC after culture (dark blue arrow).

high swelling ratio in PBS (pH 7.4) at 37 °C, which allows them to absorb wound exudates and release drugs (Fig. 2N). The pore size, porosity, and swelling ratio results suggest that the PRP gel would require further improvement in crosslinking density before it could serve for chronic wound treatment. Herein, this improvement was achieved by adding SP to PRP, which significantly improved the network structure of PRP to a level suitable for chronic wound dressing applications.

3.2. Physicochemical and rheological characterization of the hydrogels

The chemical groups present in several gels were identified using Fourier transform infrared (FTIR) spectroscopy (Fig. 2Q). The PRP, SS, and SF components display similar IR absorption bands of interest for this study, including amide I (C═O at 1656 cm^{-1}), amide II (N–H at 1534 cm^{-1}), amide III (C–N at 1239 cm^{-1}), and –OH stretching at 3290 cm^{-1} [37]. The FTIR spectrum for SP@PRP comprises peaks characteristic for peptide (amide) bonds, including amides I, II, and III, with a shifted and increased intensity –OH stretching band due to free hydroxyl groups relatively to SS and SF, suggesting that covalent bonding was more prevalent and hydrogen bonding was decreased in fibrin network formation. The shift in the amide I (C═O) band from 1656 to 1637 cm^{-1} in the SP@PRP spectrum is also consistent with the presence of ionic interactions between Ca^{2+} and SP [64,65]. Ellerbrock et al. indeed showed that Ca^{2+} caused shifting of the C═O absorption band towards lower wave number (WN) values in poly(galacturonic acid)-Ca^{2+} mixtures [65]. It was pointed out that cations such as Ca^{2+} may interact with

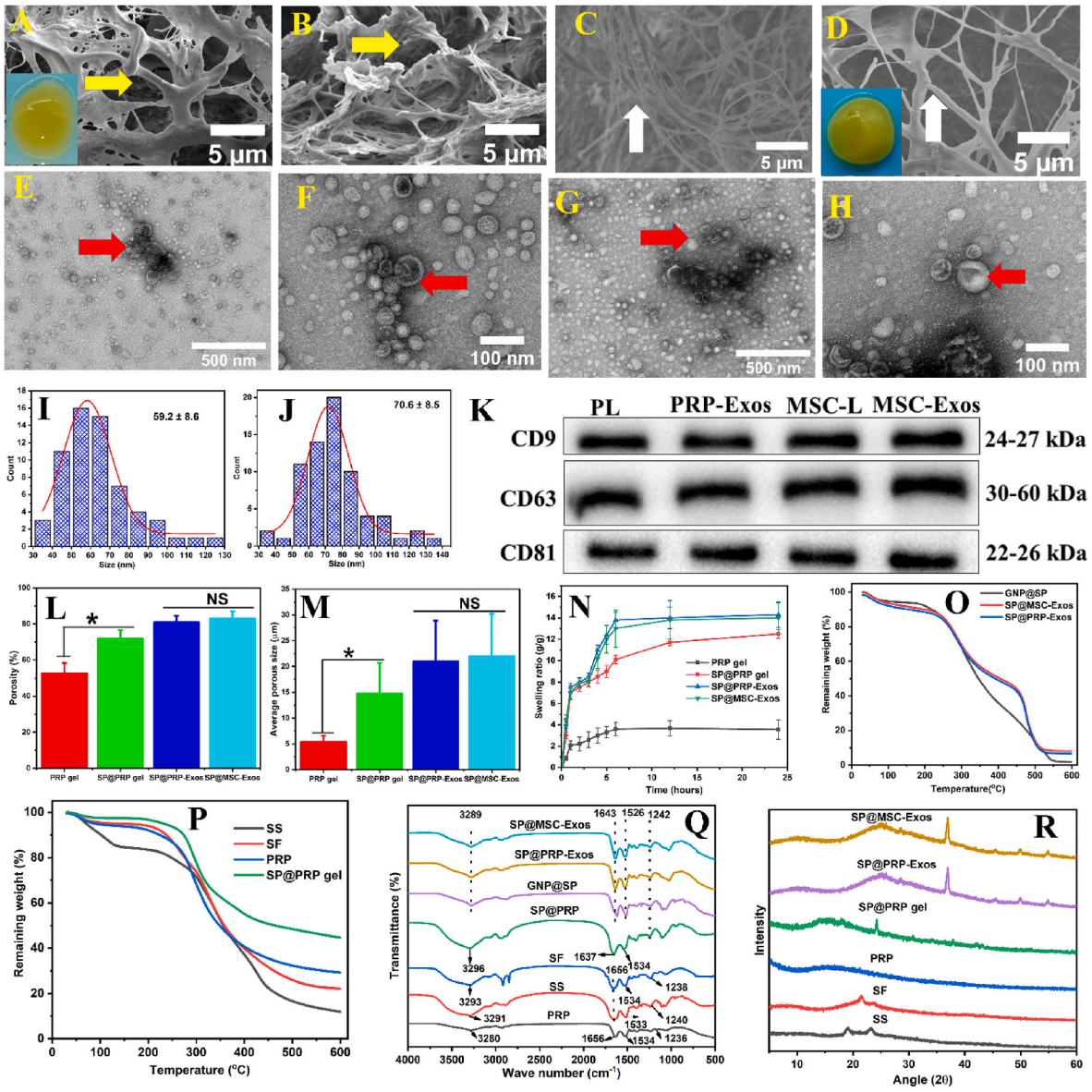

Fig. 2. Characterization of gel samples. FESEM imaging of (A) PRP gel and (B) SP@PRP gel shows that the gels have a network-like porous structure (yellow arrow). Cross-sectional FESEM images for the PRP gel (C) and the SP@PRP gel (D), showing randomly ordered fibril elements of different thicknesses (white arrows) at 5000 × magnification. The insets show the visual appearance of the PRP gel and SP@PRP gel. Typical TEM images for PRP-Exos (E–F) and MSC-Exos (G–H), with visible exosome structures (red arrows). Size distribution diagram for the exosomes in PRP-Exos (I) and MSC-Exos (K), measured in the TEM images with ImageJ. (K) Western blot analysis of the surface biomarkers CD9, CD63, and CD81 in PRP-Exos and MSC-Exos. PL, platelet lysate; MSC-L, MSC-lysate. (L) Porosity, (M) average pore size, (N) swelling ratio, (O–P) TGA, (Q) FTIR, and (R) XRD analysis of different gels. Data are presented as the average value ± standard deviation (SD) ($n = 3$). NS indicates no significance, and * indicates $P < 0.05$.

aldehyde, carboxylic acid, ketone and ester functionalities (all containing C═O bonds), as well as amide (CO–NH), carboxylate (COO^-) and hydroxyl (OH) functional groups [64,65]. These groups are either fully negatively charged, such as carboxylate ions, or partially negatively charged, such as amides, aldehydes, carboxylic acids, ketones, and esters, and thus contribute to the interactions with the Ca^{2+} cation. These interactions influence the strength of the double bond between the C and O atoms in the carbonyl groups [65]. We found that Ca^{2+} affected the C═O absorption bands, in agreement with previous studies [66]. Thus, the SP@PRP dual-crosslinked hydrogel involved covalent bonding mediated by thrombin, and ionic bonding by Ca^{2+}, in addition to H-bonding present in the β-sheet structures of SF.

The incorporation of the covalent crosslinker genipin (GNP) was demonstrated by the characteristic C═O (amide I) and N–H (amide II) stretching bands shifting from 1656 and 1534 cm^{-1} to 1643 and 1526 cm^{-1}, respectively, in GNP@SP, SP@PRP-Exos and SP@MSC-Exos. In a study by Bao et al., the amide I and II bands were shown to shift to lower WN values in SF-based hydrogels due to the formation of an amide bond between the ester group of GNP and the NH_2 groups of SF [67]. Arjeh et al. also demonstrated that after GNP crosslinking of spirulina protein-based hydrogels, a significant shift in the amide II band from 1529 to 1501 cm^{-1} was observed [68]. The absorption band shifts were associated with the production of secondary amides by the reaction between GNP and the primary amino groups of proteins [69]. Moreover, herein, the GNP addition reduced the intensity of the amide I and II bands due to crosslinking involving amide groups, as shown in previous studies [70]. The amide III band also shifted slightly from 1238 to 1242 cm^{-1} when SP, SP@PRP-Exos, and SP@MSC were crosslinked with GNP. Indeed, Imsombut et al. showed that crosslinking of SF with GNP induced amide III band shifting to higher WN values [71], which

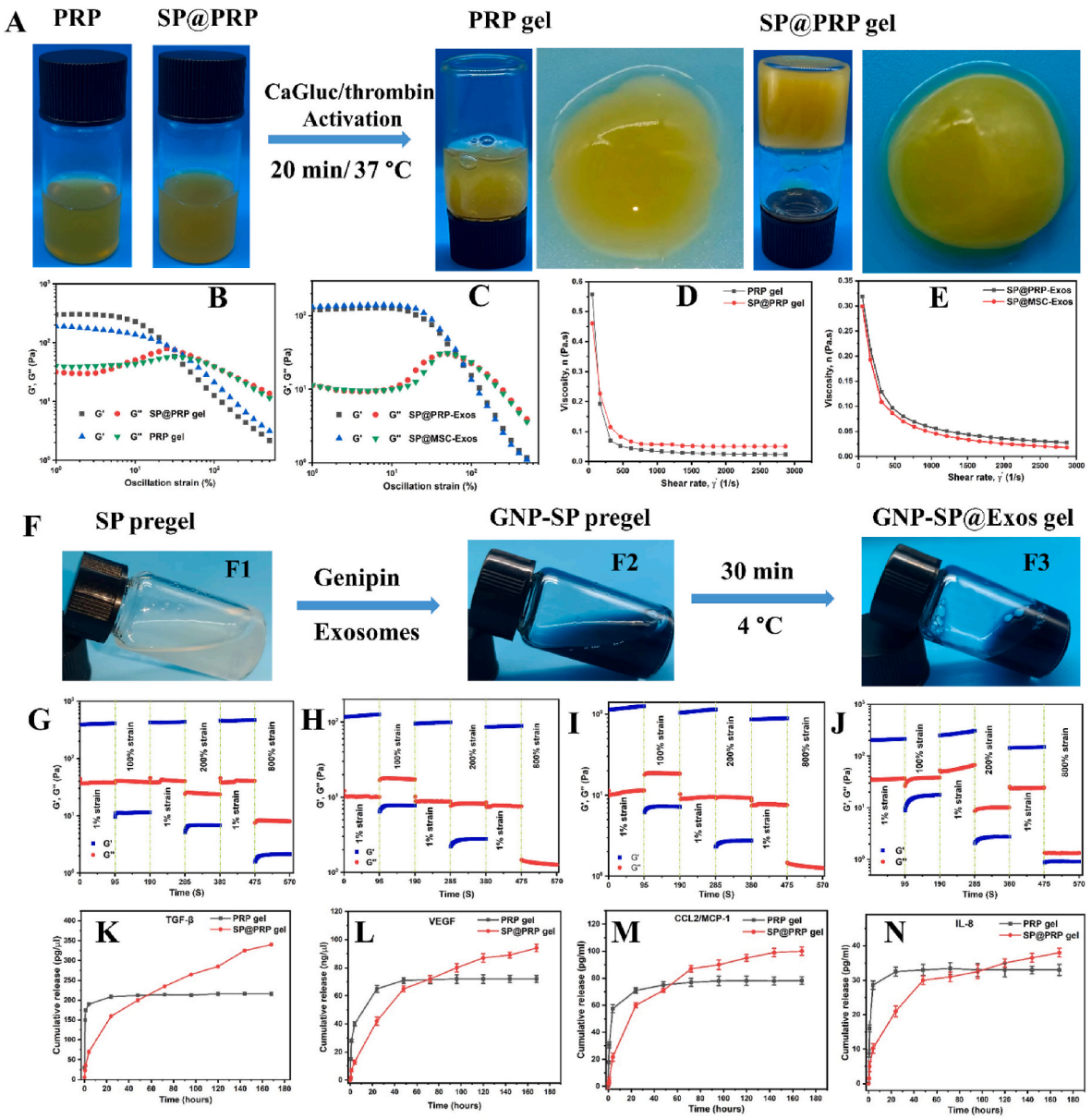

Fig. 3. Appearance, rheology, and release properties of the gels. (A) Fabrication and macroscopic appearance of PRP and SP@PRP gel activated with a calcium gluconate (CaGluc)/thrombin mixture. Strain sweeps for (B) PRP and SP@PRP gels, (C) SP@PRP-Exos, and SP@MSC-Exos. Shear rate-dependent viscosity for (D) PRP gel and SP@PRP gel, (E) SP@PRP-Exos and SP@MSC-Exos. (F) Preparation of SP@PRP-Exos and SP@MSC-Exos gels. (F1) Silk protein pre-gel at 2%, (F2) exosome-loaded genipin-crosslinked silk protein pre-gel, (F3) exosome-loaded genipin-crosslinked silk protein gel (SP@PRP-Exos and SP@MSC-Exos). Alternating strain sweeps for (G) PRP gel, (H) SP@PRP gel, (I) SP@PRP-Exos, and (J)SP@MSC-Exos. Release of (K) transforming growth factor-β (TGF-β), (L) vascular endothelial growth factor (VEGF), (M) monocyte chemoattractant protein 1(MCP 1), and (N) interleukin-8 (IL-8) from PRP and SP@PRP gels after immersion in fresh DMEM without antibiotics and FBS, incubated at 37 °C with 5% CO_2 for up to 7 days. Data are presented as the average value ± standard deviation (SD) ($n = 3$).

suggests that SF structures transitioned from predominantly random coil to β-sheet conformations [71]. Furthermore, the broad absorption band from 3280 to 3300 cm^{-1}, characteristic for hydroxyl stretching vibrations and strongly influenced by H-bonding, is weakened and shifted to lower WN values in SP@PRP-Exos and SP@MSC-Exos relatively to SS and SF, suggesting the enhanced formation of inter- and intramolecular hydrogen bonds. After blending GNP@SP with PRP-Exos and MSC-Exos, the OH and amide I, II, and III bands were not significantly affected, suggesting that the exosomes did not affect the inherent structure of GNP@SP. SP@PRP-Exos and SP@MSC-Exos dual-crosslinked hydrogels involve covalent bonding and enhanced H-bonding, both mediated by GNP. Therefore, all these characteristic peaks confirm that the dual-crosslinked hydrogels were successfully synthesized. XRD analysis (Fig. 2R) showed that SS was amorphous, as demonstrated by two broad bands at $2\theta = 19.08$ and $23.86°$. Pure SF displays a small peak at $2\theta = 22.2°$ without prominent strong peaks, signifying that it exists primarily in the random-coil conformation, while PRP has no apparent peaks. As evidenced by the broad diffraction peaks at $2\theta = 15.08$ and $24.6°$, the incorporation of SP in PRP increased the crystallinity of PRP. After adding GNP to SP, crosslinked SF is detected through a prominent peak at $2\theta = 26°$ and a weaker peak at $2\theta = 36°$. These findings are consistent with the FTIR results showing that SS, SF, and exosomes were effectively combined and crosslinked with GNP. This change in the secondary structure of SF from random coils to β-sheets confirms that its crystallinity was improved. The XRD and FTIR results suggest that crosslinking with GNP produced bonds that can potentially enhance the physical properties of the hydrogels.

In TGA measurements (Fig. 2O-P), the SP@PRP dual-crosslinked

hydrogel exhibited higher thermal stability than the SS, SF, and PRP gels. Additionally, the presence of PRP-Exos and MSC-Exos affected the thermal stability of GNP@SP slightly, with the decomposition curves shifting towards higher temperatures. This improved thermal stability would enable wound dressings to resist thermal degradation better when applied to hyperthermic wounds.

The mechanical properties of different hydrogel systems, PRP gel versus SP@PRP gel and SP@PRP-Exos versus SP@MSC-Exos, were compared at 37 °C using rheological tests, including strain sweeps, alternate strain sweeps, and viscosity measurements (Fig. 3B–E). For all the gels, the storage modulus (G′) was larger than the loss modulus (G″), signifying that the elastic properties dominated over the viscous properties, yielding low tan delta values making these materials suitable for injection, drug delivery, and tissue regeneration [72]. Furthermore, as expected, the SP@PRP gel outperformed the PRP gel in terms of mechanical behavior, indicating that dual-crosslinking between Ca^{+2} and SP also contributed to the overall mechanical performance (Fig. 3B), whereas SP@PRP-Exos and SP@MSC-Exos had nearly identical G′ and G″ values, demonstrating that the exosomes did not affect the rheological properties of the gels (Fig. 3C). G′ and G″ were monitored by cycling the strain three times between 1 and 800%, to assess the self-healing and shear thinning behaviors of the different gels, critical for clinical hydrogel dressings. A significant decrease in G′ and G″, with G′ decreasing dramatically and instantly below G″, was observed when the gels were subjected to high strains (100, 200 and 800%) for all the samples, demonstrating the excellent shear thinning capacity of the gels. G′ and G″ also recovered their original values at low shear strain (1%) after three strain sweep cycles, indicating their excellent self-healing ability (Fig. 3G–I). This suggests that the gels could easily conform to the shape of wounds, which is advantageous in wound management. Furthermore, the viscosity of the gels decreased as the shear rate was increased, further demonstrating the shear thinning performance of the gels, which would be beneficial in extrusion-based injection operations. The viscosity of the dual-crosslinked hydrogels at the lowest shear rate examined (50 s^{-1}) reached values of 0.48 Pa s for the PRP gel, 0.56 Pa s for the SP@PRP gel, 0.30 Pa s for SP@MSC-Exos, and 0.33 Pa s for SP@PRP-Exos (Fig. 3D–E). Due to the rates of hydrogen bond formation and breaking becoming equal during gel flow, the viscosity of all the gels remained almost constant (0.02 Pa s) at higher shear rates (>1500 s^{-1}). These findings demonstrate that these dual-crosslinked hydrogels could serve to fill wound areas via injection or smearing, which may facilitate various types of clinical practices.

3.3. Determination of protein released from dual-crosslinked hydrogels

The concentration of GFs and cytokines in PRP gel and SP@PRP gel was determined using ELISA kits at various time intervals after immersion in DMEM without antibiotics and serum (Fig. 3K-L). The platelets contain many granules with bioactive factors, proteins, and hormones that are released when activated by various agonists. The *in vitro* studies revealed that the SP@PRP gel released sustainably more VEGF, TGF-β, IL-8, and CCL2/MCP-1 over time than the PRP gel. The release of cytokines and GFs from the gels is partly regulated by diffusion. Initial burst release of the GFs and cytokines was noticed, followed by controlled release; an average of 12, 53, and 73% of the loaded GFs and cytokines were released from the SP@PRP gel versus 50, 94, and 100% from PRP after 1, 24, and 48 h, respectively. When PRP is activated, platelet GFs are released all at once, so the activity timeframe is too limited to regenerate most damaged tissues. Additionally, the total protein content (exosomes and SP) was progressively released from SP@PRP-Exos and SP@-MSC-Exos (Fig. S11). In these dual-crosslinked hydrogels, sustained release supplanted burst release. Exosomes and SP can contribute significantly to several wound healing stages [37,73]. Thus, the gradual release of exosomes and SP will extend their influence in various stages of wound healing, resulting in effective tissue regeneration and remodeling.

This study showed that (i) the release of the target biomolecules changed over time, with concentrations and kinetics mainly increasing up to 7 days of incubation for the dual-crosslinked hydrogels; (ii) the release kinetics were generally biomolecule-dependent, as was also shown in other studies [74]; and (iii) the combination of PRP or exosomes with SP promoted the long-term release of biomolecules.

3.4. Improvement of biodegradability

An essential characteristic of biomaterials is biodegradability, because it impacts the regeneration of tissues, in particular the development of primary regenerating tissues and subsequent remodeling [75]. We examined the biodegradability of different gels immersed in PBS (pH 7.4) at 37 °C at predetermined time intervals, to characterize the gels further. The results in Fig. 4A show that the SP@PRP gel degraded by about 21% after two days, as compared to 50% for the PRP gel, indicating that the addition of SP into the PRP networks significantly decreases their degradation rate. The same trends were observed for SP@PRP-Exos and SP@MSC-Exos (Fig. S12). Thus, dual-crosslinking produced the best scaffolds in terms of degradability, given that more sustained release of GFs is expected for longer degradation times. This is consistent with the above results for the release assays.

Considering their biodegradation rate, in the *in vivo* animal studies, all the gels were renewed every two days to maintain a steady release of bioactive substances, while enabling an adequate time frame for diabetic wound healing.

3.5. Antibiofilm and antimicrobial activity of the gels

In clinical studies, half of diabetic wounds are generally colonized by skin microbiota within a few days. Within one to four weeks, unique species of Gram-positive bacteria (beta-hemolytic streptococci and *S. aureus*) take over, causing a purulent discharge that is clinically important [4,5]. After 4 weeks, the diabetic wound is colonized by polymicrobial mixtures of aerobic and anaerobic pathogens, resulting in tissue necrosis and extensive ulceration [4,5]. Moreover, 15% of diabetic wound infection patients require lower limb amputation to prevent infection spread [76]. Diabetic foot osteomyelitis (DFO) represents the most common infection related to diabetic foot ulcers, occurring in 50%–60% of serious infections, and is responsible for elevated amputation rates [77]. The DFO is typically the result of an infection of the soft tissues that extends into the bone, damaging the cortex and, eventually, the marrow [78]. Further, it was shown that microbial biofilms associated with infectious bone disease can resorb HA, the inorganic bone component, in the absence of host immunity [79]. Therefore, we hypothesized that the dual-crosslinked hydrogels could eradicate microbial biofilms on HA. Thus, we constructed an *in vitro* experiment with microbial biofilms involved in DFO to test this hypothesis. The results obtained show that all the microbial biofilms were able to alter the HA surfaces (Fig. 4D–K) as compared with the control (Fig. 4C and S13), with the most extensive damage caused by MRSA. This indeed suggests that bacteria infecting diabetic wounds have the ability to resorb bone tissues in the absence of host immunity, which can potentially lead to amputation. Interestingly, the results also indicate that dual-crosslinked hydrogels eradicated microbial biofilm growth on HA for all the bacteria tested, including MRSA, E. coli, and P. aeruginosa (Fig. 4F, I, and L). Hence, the dual-crosslinked hydrogels should be able to eliminate microbial infection and the risk of infection-related amputation in diabetic wounds. Furthermore, the antimicrobial activity of PRP and different gels, including the PRP gel, SP@PRP gel, SP@PRP-Exos, and SP@MSC-Exos, was established using the agar well diffusion and disk diffusion methods with E. coli, P. aeruginosa, S. aureus, and MRSA (Fig. 4M – N, S14, and S15). Since the antibacterial activity of azithromycin (AZM) against both Gram-positive and Gram-negative bacteria is well-established [80], it was used as a positive control.

The PRP (without activators) and SP@PRP gel both displayed

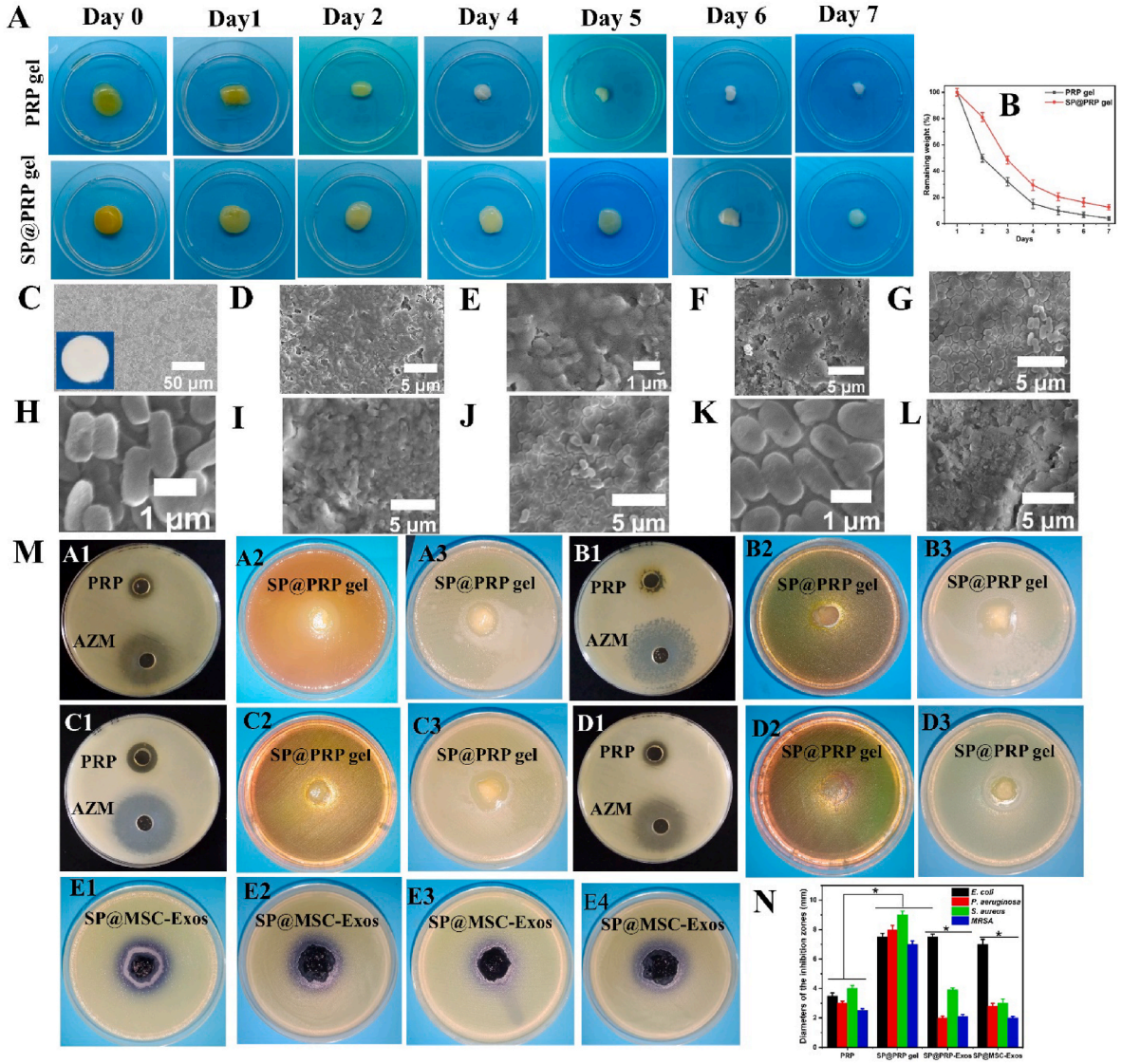

Fig. 4. Degradation and antimicrobial activity of gels. (A–B) Degradation behavior of PRP and SP@PRP gels treated with calcium gluconate/thrombin after immersion in PBS at 37 °C. (C–L) FESEM images of HA discs, microbial biofilm-induced alteration on HA disc surfaces, and antibiofilm activity of the dual-crosslinked hydrogels on biofilm-covered HA discs: (C) the intact surface of sintered HA. The inset shows the naked-eye appearance of the HA disc, with a regular, smooth surface and no internal defects nor evidence of porosity. (D–E) MRSA biofilm-induced alteration on HA; (F) MRSA biofilm treated with gel; (G–H) P. aeruginosa biofilm-induced alteration on HA; (I) P. aeruginosa biofilm treated with gel; (J–K) E. coli biofilm-induced alteration on HA; (L) E. coli biofilm treated with gel. (M) Agar-well diffusion experiments to illustrate the formation of inhibitory zones for PRP against (A1) *E. coli,* (B1) *P. aeruginosa*, (C1) S. aureus, and (D1) MRSA. Azithromycin (AZM) served as positive control. The formation of inhibitory zones is observed for the SP@PRP gel against *E. coli* cultured on MAC (A2) and MHA (A3), *P. aeruginosa* cultured on MAC (B2) and MHA (B3), and *S. aureus* cultured on MSA (C2) and MHA (C3). MRSA was cultured on MSA (D2) and MHA (D3). The formation of inhibitory zones is observed for SP@PRP-Exos against *E. coli* (E1) and *P. aeruginosa* (E3), and for SP@MSC-Exos against *E. coli* (E2) and *P. aeruginosa* (E4). (N) Diameter of the inhibition zones. *P < 0.05. PRP, platelet-rich plasma; SP, silk protein; PRP-Exos, platelet-rich plasma exosomes; MSC-Exos, mesenchymal stem cell-derived exosomes; MAC, MacConkey agar; MHA, Muller Hinton Agar; MSA, Mannitol Salt Agar. Data are presented as the average value ± standard deviation (SD) ($n = 3$). NS indicates no significance, and * indicates $P < 0.05$.

antibacterial activity against all the tested bacteria, with the highest inhibition observed against S. aureus (4.0 ± 0.2 mm for PRP and 9.0 ± 0.3 mm for the SP@PRP gel), *and the* lowest inhibition against MRSA (2.5 ± 0.1 mm for PRP and 7.0 ± 0.2 mm for SP@PRP gel). Bielecka et al. found similar results, reporting that PRP inhibited the growth of MRSA and methicillin-sensitive Staphylococcus aureus (MSSA) [81]. More interestingly, the antibacterial activity displayed against MRSA indicates that the gels can eradicate MRSA infections, which are found in 10–32% of diabetic wound infections and are linked to increased probability of therapeutic failure, disability, and hospitalization expenses [82]. Furthermore, diabetes patients with MRSA infections die at a rate five times higher than those without MRSA infections [76]. The SP@PRP gel inhibited the growth of *S. aureus*, which is the most commonly isolated pathogen in diabetic wounds [82]. The SP@PRP gel also displayed antibacterial activity against P. aeruginosa *and* E. coli, which frequently cause diabetic wound infections and delay healing [81, 83].

The antimicrobial properties of PRP are due to various factors [84]: (i) the release of GFs-platelet antimicrobial proteins such as platelet factor 4 and RANTES (Regulated on Activation Normal T Cell Expressed and Secreted), which are effective against Gram-positive bacteria such as MRSA and MSSA, Gram-negative bacteria such as *E. coli*, and fungi such as Candida albicans, *as well as viruses*. Moreover, oxygen metabolites (hydrogen peroxide, superoxide, and hydroxyl free radicals)

released after platelet degradation directly attack bacteria and aid in pathogen attachment, aggregation, and absorption to increase clearance; (ii) antimicrobial peptides-host defense peptides such as defensins and cathelicidins, that are generated continuously by cells such as leukocytes; and (ii) plasma, comprising a complementary system that can be activated to enable microbial cell lysis. The antibacterial peptides have a destructive effect on bacterial cell membranes, which they enter. These generalized antimicrobial pathways lower the probability that bacteria acquire resistance to PRP, in contrast to antibiotics that selectively target specific components of bacterial cells [85].

Differences in antibacterial activity between PRP, PRP gel and SP@PRP gel were highly significant, suggesting that platelet activation by CaGluc and thrombin increased the antibacterial activity, while there was no statistical difference between the PRP gel and SP@PRP gel in terms of antibacterial activity, suggesting that the added SP (SF and SS) did not affect significantly the antibacterial activity of the gels. SF does not exhibit antimicrobial properties, while the activity of SS depends on its concentration, source, and extraction method [63]. The SP@PRP-Exos and SP@PRP-MSC displayed antimicrobial activity against all the microorganisms tested. The highest antibacterial activity (7.0 ± 0.4 mm inhibition zone) was detected against E. coli, and the lowest activity (2.0 ± 0.1 mm inhibition zone) against MRSA. These findings show that SP in combination with exosomes efficiently inhibited the proliferation of the tested microorganisms.

Considering all the results of the antimicrobial tests, we conclude that the prepared dual-crosslinked hydrogels possess *in vitro* antibacterial activity potent enough to treat diabetic wound infections in the clinic.

3.6. Gel culture under inflammatory conditions

In vitro, lipopolysaccharides (LPS) stimulate inflammatory cells such as macrophages. Therefore, the response of murine macrophage-like cells (RAW 264.7) to treatment with PRP, SP@PRP gel, SP@PRP-Exos, and SP@MSC-Exos was evaluated under inflammatory conditions (Fig. 6A–E). The gels were incubated with macrophages and LPS for 24 h, and ELISA was used to determine the release of anti-inflammatory (IL-10 and IL-4) and pro-inflammatory (IL-1 and TNF-α) cytokines from the media conditioned with the different gels. The purpose of this test was to evaluate the anti-inflammatory activity of the gels, by simulating chronic wound environments where the long-lasting inflammation phase is the main factor slowing healing. Under such conditions, pro-inflammatory cytokines such as IL-1β (16 ± 6 ng/mL) and TNF-α (550 ± 80 pg/mL) were released at concentrations higher in the control than in the different gel treatment groups (<2 ng/mL for IL-1β and <50 pg/mL for TNF-α). In contrast, anti-inflammatory cytokines, including IL-4 (5.0 ± 0.2 ng/mL) and IL-10 (4 ± 2 pg/mL) in the control were significantly lower than in the other groups (>8 ng/mL for IL-4 and >16 pg/mL for IL-10, Figs. S16B–E). Moreover, no significant difference was detected for cytokines released from the different gels, suggesting that the dual-crosslinked hydrogels inhibit inflammation. This is evidenced by the rise in anti-inflammatory cytokines and the decrease in pro-inflammatory cytokines. Macrophage staining also confirmed this with anti-CD86 and anti-CD206 antibodies (Fig. S16A). CD86 is associated with M1 macrophage polarization, while M2 macrophage markers comprise CD206 [86]. Macrophages play a crucial role in regulating the wound healing process. As the wound heals, their phenotype changes from M1 to M2 macrophages, indicating a differentiation potential that alters their role from promoting inflammation to promoting proliferation [87]. M1 macrophages predominate during the pro-inflammatory phase of wound healing, and their strongly phagocytic nature serves to clean and remove dead tissues from the wound [87]. M2, on the other hand, has been linked to an anti-inflammatory role and functions in angiogenesis and tissue repair [88]. Diabetes wounds are M1-excessive in the initial stages but M2-deficient in the later proliferative phase, which indicates that changes in macrophage activation are potentially contributing to diabetic wound healing impairment [89]. Therapies targeting the reversal of this abnormal activation could be used to enhance the wound healing process [89]. Herein, most macrophages in the LPS samples were stained with CD86, defining M1 macrophages, whereas most macrophages in the dual-crosslinked hydrogels were stained with CD206, expressing M2 macrophages. Furthermore, a roughly spherical cell shape, typical for the monocyte morphology, was noted for the LPS (Fig. S17A). In comparison, the dual-crosslinked hydrogels included some elongated cells, indicating a greater M2 macrophage polarization potential. Due to the phenotypic transition between M1 and M2, some macrophages can express M1 and M2 markers at the same time [90]. By inducing early M2 macrophage polarization, the dual-crosslinking hydrogels reduce the inflammation phase and accelerate the diabetic wound healing process.

Pro-inflammatory cytokines such as IL-1β and TNF-α are thought to be the primary pathological causes of wound healing delay [91,92]. TNF-α induces fibroblast apoptosis, reduces fibroblast proliferation, and impairs keratinocyte migration, thereby delaying diabetic wound healing [92]. IL-1β induces prolonged wound healing in diabetic patients by altering the ECM and regulating MMP-2 and MMP-9 via the p38 pathway [91]. Therefore, targeting pro-inflammatory cytokines represents an important therapeutic strategy for enhancing diabetic wound healing.

In conclusion, the dual-crosslinked hydrogels generate a more anti-inflammatory environment associated with reduced cell inflammation, which is crucial for tissue regeneration.

3.7. Cell proliferation and migration

Cell viability was evaluated using NIH-3T3 and HUVEC cells with the CCK-8 assay as previously described [36]. The viability of cells in contact with the PRP gel, SP@PRP gel, SP@PRP-Exos, and SP@MSC-Exos was significantly greater than for the control (medium) ($P < 0.05$), suggesting that all the gels were non-toxic and increased cell proliferation, which is beneficial to wound healing (Fig. 5A, C, D). Live/dead staining also confirmed the non-toxic nature of the gels: No dead cells were observed in any sample. The evaluation of *in vitro* cell migration for NIH-3T3 cells is illustrated in (Fig. 5B, E). The migration rate of the cells on PRP gel, SP@PRP gel, SP@PRP-Exos, and SP@MSC-Exos after 24 h was 63 ± 3%, 68 ± 5%, 66 ± 3%, and 65 ± 4%, respectively, as compared to 41 ± 4% for the control. This shows that NIH-3T3 cells cultured with the gels displayed a significantly greater migration rate 24 h after the beginning of wound healing than the control cells (medium), and that the cells contacted each other on both sides after 48 h, while in the control, the migration rate was still 82 ± 4%. These results demonstrate that PRP, exosomes, and SP play vital roles in improving the proliferation and migration of cells. PRP and exosomes appear to activate a group of GFs and adhesion receptors promoting cell proliferation and migration [93], whereas SF activates the traditional NF-kB signaling pathway, which leads to increased expression of various GFs inducing cell proliferation and migration [40].

3.8. Dual-crosslinked hydrogel-promoted diabetic wound contraction

The above investigations allowed us to establish that the dual-crosslinked hydrogels exhibited suitable storage modulus, shear thinning, self-healing, porous structure, porosity, swelling ratio, thermal stability, and biodegradability to serve as carriers for bioactive agents with antibacterial activity, anti-inflammatory properties, promoting cell proliferation and migration for both endothelial and fibroblast cells. An evaluation of the dual-crosslinked hydrogels to accelerate diabetic wound healing *in vivo* was then performed. We hypothesized that the increased proliferative and migratory effects observed in cell cultures *in vitro* would further translate into accelerated diabetic wound closure *in vivo*. At the same time, the anti-inflammatory and antibacterial properties of these materials should shorten the inflammation phase, as well

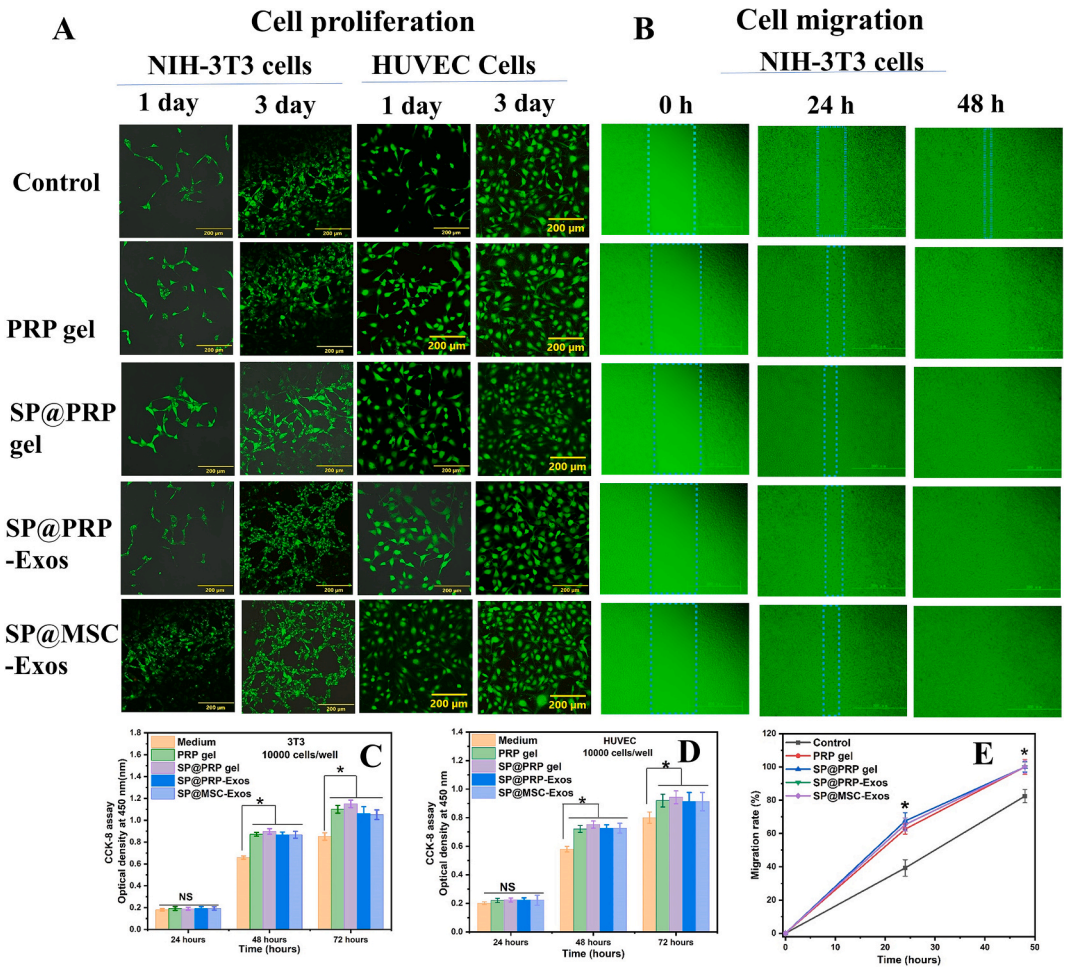

Fig. 5. *In vitro* biocompatibility of gels and **wound healing insert (culture-insert) to detect cell migration. (A)** Live/dead staining of NIH-3T3 cells and HUVEC cells. **(B) Migration states for control (culture medium), PRP gel, SP@PRP gel, SP@PRP-Exos, and SP@MSC-Exos.** Viability of (C) NIH-3T3 and (D) HUVEC cells cultured in sample extracts**.** ($P < 0.05$). Data are presented as the average value ± standard deviation (SD) ($n = 3$). NS indicates no significance, and * indicates $P < 0.05$.

as prevent bacterial infection and wound ulceration. A full-thickness chronic diabetic wound model was developed in SD rats, and the effects of the dual-crosslinked hydrogels on the wound healing process were assessed. In brief, the *in vivo* experiments were divided into two steps of two weeks each (Fig. 6A–B and Fig. S18). After diabetes induction and wounding on the right side of the rat's back, 38 rats were assigned to the SP group, the PRP gel group, and the dual-crosslinked hydrogel groups, including the SP@PRP gel group, SP@PRP-Exos group, and SP@MSC-Exos group, and 6 rats were assigned to the diabetic control group. After a blood crossmatch test, the dressings were replaced every two days post-surgery, and the wounds were covered with Tegaderm™ Film and sterilized bandages. On the 14th POD, the rats were subjected to new wounding on the left side of their backs, and the treatments were alternated between groups based on their composition (PRP gel vs SP@PRP gel, SP@PRP-Exos, and SP@MSC-Exos).

The wounds were subjected to macroscopical and histological assessments. Gross observations of the diabetic wounds for both steps were noted on days 0, 3, 7, 10, and 14. The resulting photographs are provided in Fig. 6C, F, and Fig. S18. The most crucial aspect of wound healing is wound closure, since a closed wound can act as a barrier for the skin and prevent bacterial infection. On the 3rd POD, there were no significant variations in WHR among the groups. However, the results revealed significantly superior wound contraction in the dual crosslinked hydrogel groups on days 7 ($P < 0.01$), 10 ($P < 0.5$) and 14 ($P < 0.5$) as compared with the SP gel, PRP gel, and diabetic control groups ($P \leq 0.5$, Fig. 6D–E and Fig. S18). On the 14th POD, there was complete re-epithelialization in dual-crosslinked hydrogels with initiation of the next wound healing stage, the remodeling phase, while the diabetic control group, SP, and PRP gel groups presented 50 ± 5%, 78 ± 4% and 81 ± 5% WHR, respectively. As shown in Fig. 6D–E and Fig. S18B, there was no significant difference in WHR between the first and second steps in the analyses performed on the same rats, despite an increase in blood glucose value observed at the second step.

As a clinically approved regenerative medicine, the PRP proteins and exosomes interact and bind to particular receptors to serve as mediators increasing the expression of endogenous proteins, but proteases present in the diabetic wound bed may limit their therapeutic efficiency. Therefore, the expression of IGF-1, TGF-β1, EGF, VEGF, and MMP-9 in the newly formed skin tissues was quantified using qRT-PCR to evaluate the activity of exogenous proteins and exosomes delivered by the different hydrogels (Fig. 6G-L and Fig. S18C). During hemostasis, EGF is released by macrophages, platelets, keratinocytes, and fibroblasts [36]. The wound healing procedure was assisted through upregulated EGF synthesis, which stimulates cell motility, mesenchymal regeneration, cell proliferation, angiogenesis, epidermal cell migration into injured areas, and the deposition of constituents of the basement membrane. The expression of EGF was significantly upregulated in the PRP gel group as compared to the SP and diabetic control groups, demonstrating that the exogenous proteins released from the PRP gel improved the expression of EGF in newly formed skin tissue. During the continuous

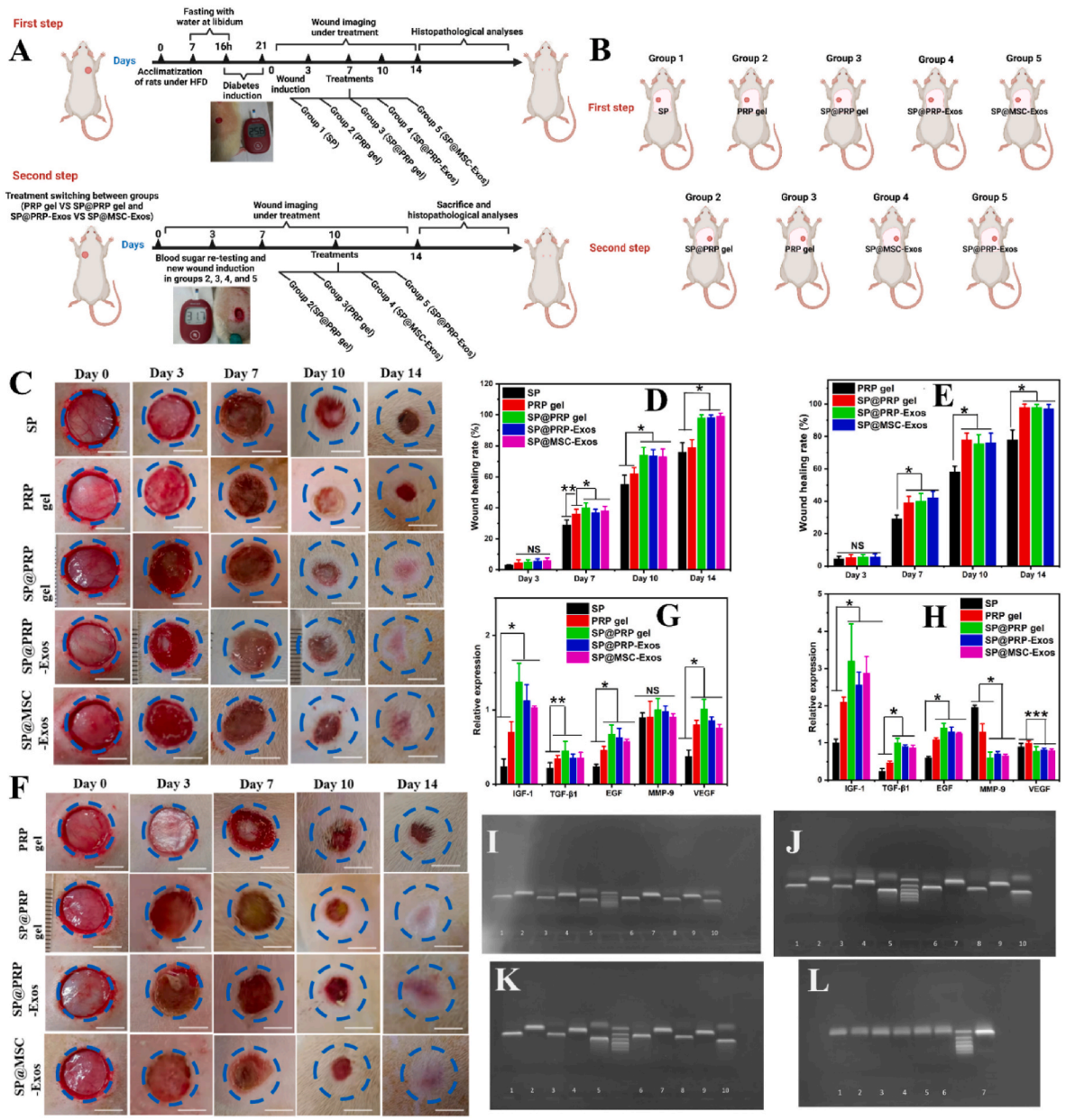

Fig. 6. Promotion of diabetic wound closure by the dual-crosslinked hydrogels (SP@PRP gel, SP@PRP-Exos, and SP@MSC-Exos). (A) *In vivo* study design for diabetic induction, and subsequent induction and healing of wounds. Diabetes was induced in the rats with an intraperitoneal injection of streptozotocin. The diabetic rats in this study had blood glucose levels above 14 mmol/L on day 21 after injection. Wounds were created 3 weeks after diabetes induction, and wound closure was monitored for two weeks. (B) Schematic illustration of treatment switching between groups. The animal study was divided into two 14-day steps, and their treatments were inversed (PRP gel vs SP@PRP gel, and SP@PRP-Exos vs SP@MSC-Exos. (C) Images of diabetic wounds in the first step with various treatment groups on days 0, 3, 7, 10, and 14. (D) Diabetic wound healing rate in the first step. (E) Images of diabetic wounds in the second step for various treatment groups on days 0, 3, 7, 10, and 14. (F) Diabetic wound healing rate in the second step. The dotted blue circles placed on the images represent the wound area on day 0. A faster rate of closure was observed for the SP@PRP, SP@PRP-Exos, and SP@MSC-Exos gels in comparison with SP and the PRP gel. Relative expressions of IGF-1, TGF-β1, EGF, MMP-9 and VEGF from skin wound tissues after 7 (G) and (H) 14 days. (I–L) Representative RT-PCR gel images for IGF (I–K 1, 6), TGF-β1 (I–K 2, 7; L7), EGF (I–K 3, 8), MMP9 (I–K 4, 9), GAPDH (I–K 5, 10), and VEGF (L1-6). Data are presented as the average value ± standard deviation (SD) ($n = 3$). NS indicates no significance, * indicating $P < 0.05$, ** indicating $P < 0.01$, and *** indicating $P < 0.001$.

wound healing phase, EGF expression in the dual-crosslinked hydrogel-treated group was highest. This increased bioactivity can be explained by the fact that PRP-proteins and exosomes are slowly released from the dual-crosslinked hydrogels, maintaining gene expression under control.

TGF-1 is a multipurpose cytokine participating in various biological functions [4]. It is released during the inflammatory stage of wound healing to induce the transformation of monocytes into macrophages, which enhances the inflammatory process and tissue clearance. As illustrated in Fig. 6G–H and Fig. S18C, on days 7 and 14, the expression of TGF-1 for the dual-crosslinked hydrogels was significantly more upregulated than in the diabetic control, as well as the SP and PRP gel groups. It was demonstrated in previous studies that in diabetic wounds, a decrease in TGF-1 levels increases the infiltration of activated inflammatory cells, thus delaying the transition from the inflammatory to the proliferative phases of the healing process [4]. Herein, the reduced inflammatory level during wound healing correlates with the higher level of TGF-1 gene expression, thereby aiding wound healing. The

findings show that the dual-crosslinked hydrogels promoted healing by greatly up-regulating TGF-1 throughout the diabetic wound healing process. TGF-1-activated fibroblasts may convert into myofibroblasts, involved in ECM deposition. Myofibroblasts express α-SMA inducing wound contraction [37]. Thus, we examined α-SMA expression by IHC at the skin wound bed. According to the quantitative assessment (Fig. S19A and Figs. S20A–B), the dual-crosslinked hydrogel groups produced significantly higher levels of α–SMA than the diabetic control, SP, and PRP gel groups ($p < 0.05$).

VEGF are among the most powerful angiogenic cytokines identified in the skin [94]. The concentration of VEGF expressed in a wound can affect the healing process significantly and facilitate the vascularization and angiogenesis stages. VEGF expression in the dual-crosslinked hydrogel group was upregulated considerably on day 7 as compared to the other groups, which illustrates their pro-angiogenic effect in the initial stage of diabetic wound healing, but it decreased slightly at day 14. In contrast, VEGF gene expression with the SP and PRP gels gradually increased on day 14. It was also higher than for the dual-crosslinked hydrogel group, demonstrating their late pro-angiogenic effect ($P < 0.01$). It was reported in previous studies that decreased VEGF mRNA levels, decreased VEGFR-2 levels, elevated VEGFR-1 levels, and aberrant sequences of VEGF receptors are primary causes of non-healing wounds [4]. Herein, the results obtained revealed that the dual-crosslinked hydrogels could initiate angiogenesis rapidly in the early stages of diabetic wound healing, achieving a physiological equilibrium between angiogenesis boosters and antagonists, progressing into the vascular stability stage, and improving blood perfusion and metabolism in the injured tissue. Restoring blood flow to wounded tissues facilitates the delivery of oxygen and nutrients for cell growth and function, accelerating wound healing [95].

IGF-1 enhanced the production of ECM and keratinocyte migration, both critical for wound epithelialization and wound contraction. A lower amount of IGF-1 in wound tissue has been reported in diabetic humans and animals as the cause of a retarded healing process [4]. On day 14, the expression of IGF-1 was higher in the dual-crosslinked hydrogel group than in the other groups. This shows that the dual-crosslinked hydrogel group could re-epithelialize faster than the diabetic control, SP, and PRP gel groups.

MMPs play essential roles in wound healing, including the clearance of degraded ECM and microbes, basement membrane degradation in capillaries for angiogenesis, keratinocyte migration, contraction, and remodeling of the scar ECM [96]. It has been shown that elevated MMPs levels are characteristic for diabetic wounds, and that the MMP concentration in chronic wounds is nearly 60 times greater than in acute wounds [4]. As shown in Fig. 6G–H and Fig. S18C, the expression of MMP-9 decreased gradually during wound healing for dual-crosslinked hydrogel groups, but increased in the diabetic control, SP gel and PRP gel groups. Chronically elevated concentrations of MMPs can destroy proteins that are not normally their substrates [96]. This can lead to the off-target breakdown of proteins, including GFs, ECM proteins and receptors, thereby hampering wound healing [97]. Similarly to our findings, it was previously demonstrated that elevated levels of MMP-9 correlate with reduced WHR [97]. Furthermore, we found that a lower MMP-9 level is linked to faster wound healing.

3.8.1. NETosis, inflammation, and oxidative stress inhibition by the dual-crosslinked hydrogels

Diabetic wounds are characterized by excessive inflammation due to neutrophil "NETs" (neutrophil extracellular traps), which delay healing. In brief, neutrophils release antimicrobial NETs composed of DNA fibers, bactericidal enzymes including myeloperoxidase (MPO), and pro-inflammatory molecules [98]. NETs thus trigger inflammation, and then capture and kill bacteria outside the cell. Unfortunately, NETs can also backfire on the host, damaging blood vessels, leading to various tissue damage, and triggering excessive inflammation [99]. In the case of diabetes, the neutrophils contain four times more of an enzyme known as PAD4, which causes the neutrophils to excrete excessive NETs [6]. Therefore, assessing markers such as MPO, which quantifies their recruitment and deposition in diabetic wound tissue, and Ly6G, NETs markers, has substantial impact on the prognosis of diabetic wound healing (Fig. 7A, C, Fig. S19D, G, and Figs. S20G–H). Quantitative analysis of MPO and Ly6G positive cell expression revealed that the dual-crosslinked hydrogel groups exhibited significantly lower MPO and Ly6G expression than the diabetic control, SP and PRP gel groups at days 7 and 14. This decrease in MPO and Ly6G matches the decrease in neutrophil NETS in the dual-crosslinked hydrogel groups, which contributed to enhanced healing as compared to the diabetic control, SP and PRP gel groups, having more neutrophils and, therefore, too many NETS. According to previous research, the amount of NETs produced is related to the degree of MPO depletion, and neutrophils deficient in MPO cannot produce NETs [100]. Moreover, neutrophil depletion in mice was previously demonstrated to enhance the re-epithelialization of uninfected diabetic wounds [6]. Overall, NETs hinder the repair process by catching too many new skin cells attempting to migrate into the wound. In this study, decreased MPO expression was also associated with decreasing MDA expression, which would reduce oxidative stress (Fig. S19B and Figs. S20C–D) [100].

Moreover, we evaluated M1 and M2 macrophage expression in skin wounds on days 7 and 14. In this investigation, we employed CD86 to characterize M1 macrophages (Fig. S19C and Fig. S20E) and CD206 (Fig. 7A and Fig. S19H) to characterize M2 macrophages. On days 7 and 14, CD86 expression in the SP and PRP gel groups was significantly higher than in the dual-crosslinked hydrogel groups. As shown in Fig. 7A and Fig. S19H, there was also a significant difference in CD206 expression between the dual-crosslinked hydrogels and the controls (diabetic control, SP and PRP gel groups). This suggests that the dual-crosslinked hydrogels have anti-inflammatory properties reducing the inflammation phase in the early wound healing stage, and accelerate the healing of diabetic wounds.

3.8.2. Formation of granulation tissue promoted by the dual-crosslinked hydrogel therapy

Granulation tissue, composed of connective tissue and blood vessels, represents the initial neotissue formed in wound healing [101]. A wound can be healed by primary or secondary intention, and wounds that heal by secondary intention are filled with a granulation tissue matrix [101]. The dual-crosslinked hydrogel groups displayed significant granulation tissue formation at the wound site on the 7th POD ($2700 \pm 200/\mu m$ for SP@PRP gel, $2200 \pm 100/\mu m$ for SP@PRP-Exos, and $2350 \pm 80/\mu m$ for SP@MSC-Exos), with more cells observed inside the tissue than in the diabetic control ($1200 \pm 100/\mu m$), SP ($1560 \pm 90/\mu m$) and PRP gel ($1800 \pm 100/\mu m$) groups (Fig. 7A–B and Fig. S18G). On the 14th POD, more granulation tissue had developed in the SP groups, and the tissue structure had also changed. There was a perceptible relative decrease in granulation tissue formed in the PRP gel and dual-crosslinked hydrogel groups, as the granulation tissue thickness decreased, suggesting further advancement in wound healing.

In addition to VEGF monitoring, the analysis of CD31, a classic indicator of endothelial cells, was performed to evaluate angiogenesis, and the ki67 marker was used for cell proliferation detection using immunohistochemistry staining on the 7th and 14th POD. Brown-labelled vessel-like structures and brown-labelled nuclei were counted in the skin tissue stained by immunohistochemistry to assess angiogenesis and cell proliferation, respectively (Fig. 7B and Figs. S19E–F). CD31 expression in the dual-crosslinked hydrogel groups ($90 \pm 10/mm^2$ for SP@PRP gel, $80 \pm 10/mm^2$ for SP@PRP-Exos, and $78 \pm 9/mm^2$ for SP@MSC-Exos) was significantly higher than in the other groups ($17 \pm 6/mm^2$ for the diabetic control group, $38 \pm 8/mm^2$ for the SP group, and $45 \pm 7/mm^2$ for the PRP gel group) at day 7 ($p < 0.5$), indicating their pro-angiogenic effect in the initial stage of diabetic wound healing following our initial VEGF evaluation. On the 14th POD, there was no significant difference among the groups. In contrast, CD31 expression in

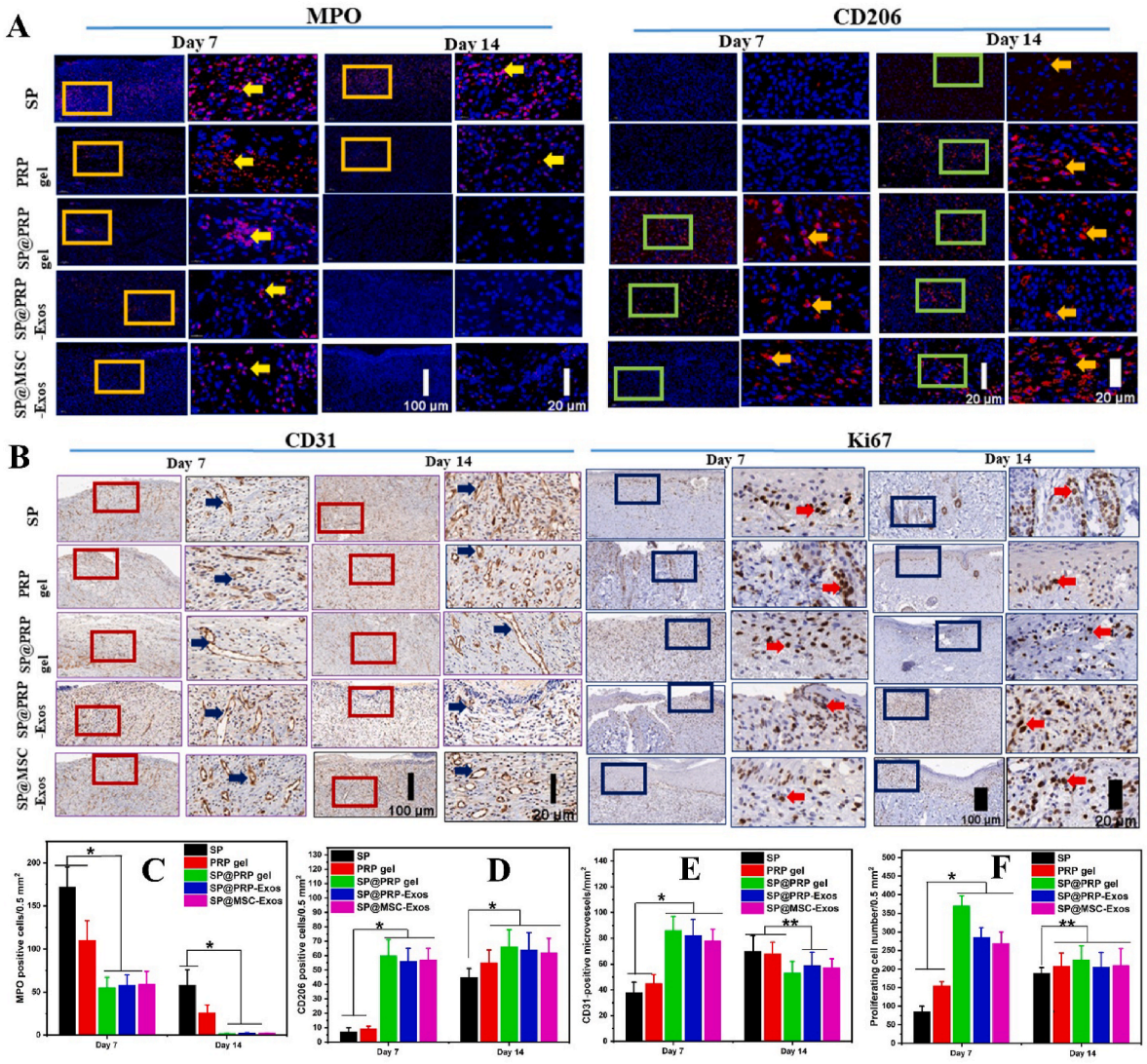

Fig. 7. Dual-crosslinked hydrogel (SP@PRP gel, SP@PRP-Exos, and SP@MSC-Exos) treatment-inhibited inflammatory response, induced angiogenesis, and enhanced cell proliferation at diabetic wound sites on days 7 and 14. (A) Immunofluorescence detection of MPO and CD206-positive cells. (B) Immunohistochemical detection of CD31 and Ki67-positive cells. (C) Statistical analysis of MPO-positive cells (n = 3). (D) Statistical analysis of CD206-positive cells (n = 3). (E) Statistical analysis of CD31-microvessels (n = 3). (F) Statistical analysis of Ki67-positive cells (n = 3). *P < 0.05, **P < 0.01.

the dual-crosslinked groups decreased, suggesting that the number of blood vessels decreased during the wound healing period, which is another indication of wound healing advancement during tissue remodeling.

Ki67 is a protein in the nucleolar cortex, produced in the nucleus during the cell cycle but not during the G0 phase (cellular quiescence state). Ki67 expression varies throughout the cell cycle but peaks during mitosis. Different proliferating cell types, such as inflammatory cells, mast cells, endothelial cells, fibroblasts, B cells, T cells, and keratinocytes, are involved in various stages of diabetic wound healing. Therefore, immunohistochemical detection of the Ki67 antigen was used to assess cell proliferation. The epidermal layer of full-thickness skin was selected for partial magnification analysis, as depicted in Fig. 7. According to the quantitative *in vitro* cytological assessment, cell proliferation was statistically significantly ($P < 0.05$) more effective in the dual-crosslinked hydrogel groups on the 7th POD (370 ± 30/0.5 mm^2 for the SP@PRP gel, 290 ± 30/0.5 mm^2 for SP@PRP-Exos, and 270 ± 30/0.5 mm^2) than in the diabetic control (68 ± 9/0.5 mm^2), PRP gel (160 ± 10/0.5 mm^2) and SP (90 ± 20/0.5 mm^2) groups, which suggests that they are better at promoting the proliferation of cells involved in skin repair. On the 14th POD, a substantial increase in Ki67-positive cells was observed in the diabetic control, SP, and PRP gel groups, suggesting a delay in cell proliferation and, therefore, the wound healing process.

Masson trichrome staining was used to identify newly formed collagen fibers within the granulation tissue. Masson trichrome stains the nuclei in black, while the keratin, cytoplasm, intercellular fibers, and muscles are stained red. Noticeably more collagen deposition was observed in the dual-crosslinked hydrogel group than the diabetic control, SP and SP@PRP gel groups on the 7th and 14th POD ($P < 0.05$, Fig. 8, and Fig. S18F). Furthermore, for all the groups, the regularity of orientation of the deposited collagen network increased with the healing time.

3.8.3. *Dual-crosslinked hydrogel therapy-promoted keratinocyte differentiation*

Epithelialization is crucial in wound healing, involving keratinocyte proliferation and differentiation [36]. K1 expression analysis (Fig. S21) and epidermal thickness (Fig. 8C and Fig. S18M) measurements were used to characterize the epithelialization of the skin wound, as K1 is a terminal differentiation marker expressed in differentiated keratinocytes [102]. On the 14th POD, the epithelial cells had covered entirely

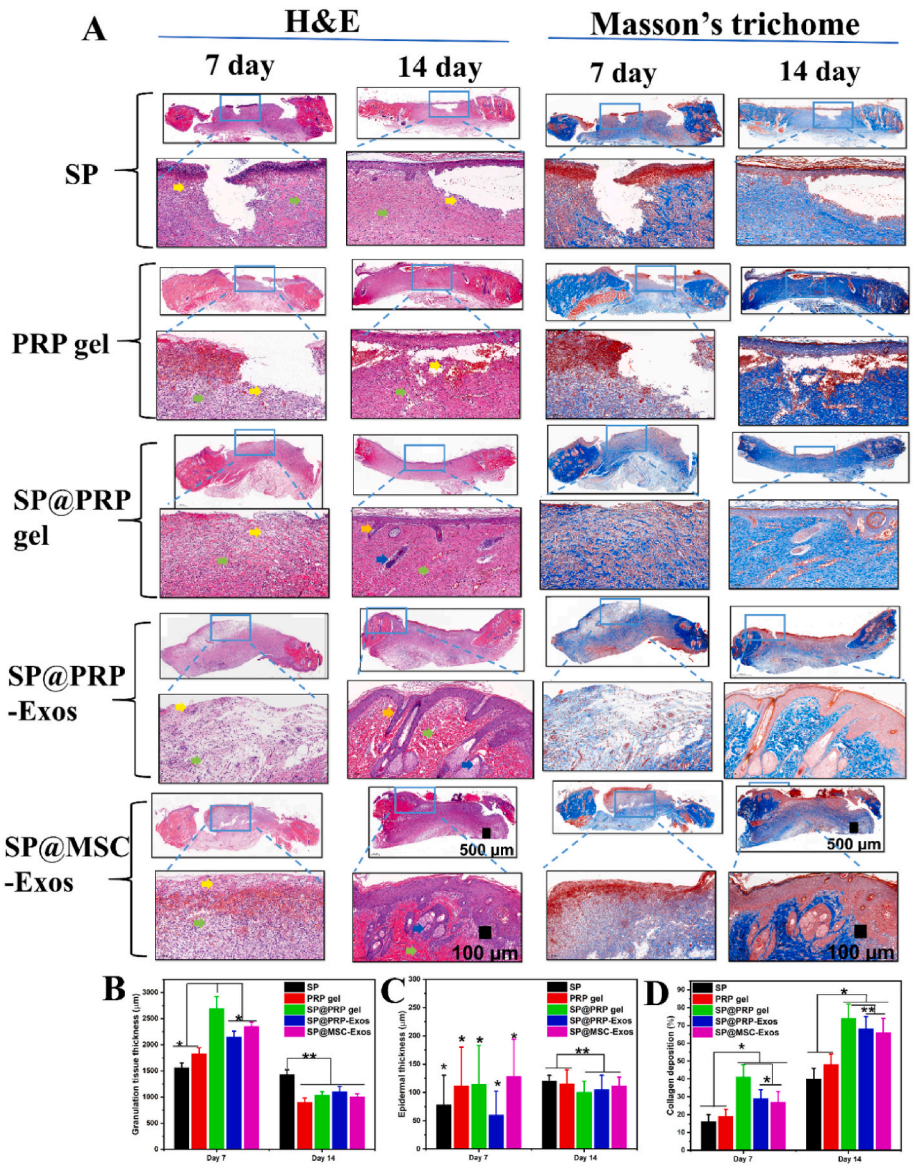

Fig. 8. Accelerated tissue regeneration with the dual-crosslinked hydrogels (SP@PRP gel, SP@PRP-Exos, and SP@MSC-Exos). (A) H&E– and Masson-stained skin tissues from treated diabetic wounds on days 7 and 14. Mature skin structures like hair follicles (orange arrows) and sebaceous glands (blue arrows) are visible for the SP@PRP, SP@PRP-Exos, and SP@MSC-Exos gel groups. In H&E, fibroblasts are indicated with blue arrows, and inflammatory cells with yellow arrows. (B) Granulation tissue thickness , (C) Epidermal thickness, (D) collagen deposition. *P < 0.05, **P < 0.01.

all the dermal tissue in the dual-crosslinked hydrogel groups, in contrast to the diabetic control, SP and PRP gel groups (Fig. S18M and Fig. S21). Furthermore, the dual-crosslinked hydrogel groups had significantly higher K1 expression than the SP and PRP gel groups ($P < 0.01$). Moreover, as compared to the SP and PRP gel groups, a perceptible increase in the number of hair follicles was noticed at the periphery of diabetic wounds treated with dual-crosslinked hydrogels.

No newborn hair follicles were noticeable at the epicenter of the wound in the diabetic control, SP, and PRP gel groups, but they were present for wounds treated with the dual-crosslinked hydrogels. Additionally, for the dual-crosslinked groups, sebaceous glands were observed both at the periphery and at the epicenter of the wound. In contrast, in the diabetic control, SP, and PRP gel groups, the sebaceous glands recovered only at the periphery of the wound.

According to the histopathological findings, the reduced ability of the PRP gel to accelerate wound healing may be due to the limited half-life of GFs combined with their fast release, which can cause them to disintegrate before reaching tissue receptors. In contrast, SP lacks GFs for direct faster healing, even though SF can stimulate the NF-kB signaling pathway, which increases the expression of various growth factors [40]. The dual-crosslinked hydrogels stimulated outstanding healing in full-thickness diabetic wounds, as demonstrated by well-organized subcutaneous tissues, the dermis, and a fully developed epidermis without scarring.

4. Conclusion

In this study, we engineered and assessed dual-crosslinked hydrogels, including SP@PRP gel, SP@MSC-Exos, and SP@PRP-Exos, to enhance synergistically diabetic wound healing. The SP@PRP gel was based upon clinically approved regenerative PRP and FDA-approved SP, using CalGluc/thrombin as activator to generate a dual-crosslinked hydrogel. The SP@MSC-Exos and SP@PRP-Exos dual-crosslinked hydrogels were based upon exosomes and FDA-approved SP, using GNP as crosslinking agent. The presence of intermolecular interactions between the gel components was confirmed by FTIR spectroscopy. The dual-crosslinked hydrogels display desirable characteristics, including self-healing, shear thinning, swelling ability, thermal stability, biodegradability, as well as anti-inflammatory properties, and the ability to promote cell proliferation and migration. Moreover, the dual-crosslinked hydrogels exhibited antibacterial activity against E. coli, P. aeruginosa, S. aureus, and MRSA. The addition of SP to PRP, PRP-Exos, and MSC-Exos improved their overall mechanical properties and prolonged the release of bioactive substances such as VEGF and TGF-β1,

resulting in a cascade of advantageous biological events and increasing their tissue regeneration potential in a diabetic wound model. The dual-crosslinked hydrogels reduced NETosis and oxidative stress, while also inducing M2 polarization, granulation tissue matrix formation, neovascularization, sebaceous gland and hair follicle regeneration, and enhanced collagen deposition, all beneficial for re-epithelialization and wound closure without scarring. Further clinical research is required to confirm the efficacy claims for these dual-crosslinked hydrogels in humans. We nevertheless propose these dual-crosslinked hydrogels as promising bioactive wound dressings for the treatment and management of chronic wounds, including infected diabetic wounds.

Ethics approval and consent to participate

All the animal experiments were approved by the Ethics Committee of the Hubei Provincial Center for Disease Control and Prevention (approval no. 202120167). All the authors were in compliance with all relevant ethical regulations.

CRediT authorship contribution statement

Bianza Moise Bakadia: Methodology, Validation, Formal analysis, Investigation, Data curation, Writing – original draft, Writing – review & editing. **Abeer Ahmed Qaed Ahmed:** Methodology, Data curation, Investigation. **Lallepak Lamboni:** Writing – review & editing. **Zhijun Shi:** Data curation, Investigation. **Biampata Mutu Mukole:** Data curation, Investigation. **Ruizhu Zheng:** Data curation, Methodology. **Mazono Pierre Mbang:** Methodology, Data curation. **Bi Zhang:** Methodology, Investigation. **Mario Gauthier:** Resources, Writing – review & editing. **Guang Yang:** Supervision, Conceptualization, Methodology, Validation, Writing – review & editing, Funding acquisition.

Declaration of competing interest

The authors declare that they have no known competing financial interests or personal relationships that could have appeared to influence the work reported in this paper.

Acknowledgements

This work was financially supported by the National Natural Science Foundation of China (51973076) and the Fundamental Research Funds for Central Universities (2020kfyXJJS035). The authors also sincerely thank the Analysis and Testing Center of Huazhong University of Science and Technology, Wuhan, China, for the characterization of various samples.

Appendix A. Supplementary data

Supplementary data to this article can be found online at https://doi.org/10.1016/j.bioactmat.2023.05.002.

References

[1] B. Giri, S. Dey, T. Das, M. Sarkar, J. Banerjee, S.K. Dash, Chronic hyperglycemia mediated physiological alteration and metabolic distortion leads to organ dysfunction, infection, cancer progression and other pathophysiological consequences: an update on glucose toxicity, Biomed. Pharmacother. 107 (2018) 306–328, https://doi.org/10.1016/j.biopha.2018.07.157.

[2] P. Saeedi, I. Petersohn, P. Salpea, B. Malanda, S. Karuranga, N. Unwin, S. Colagiuri, L. Guariguata, A.A. Motala, K. Ogurtsova, J.E. Shaw, D. Bright, R. Williams, Global and regional diabetes prevalence estimates for 2019 and projections for 2030 and 2045: results from the international diabetes federation diabetes atlas, 9th edition, Diabetes Res. Clin. Pract. 157 (2019), 107843, https://doi.org/10.1016/j.diabres.2019.107843.

[3] H.T. Sørensen, Prevention of diabetes mortality at ages younger than 25 years: access to medications and high-quality health care, Lancet Diabetes Endocrinol. 10 (2022) 151–152, https://doi.org/10.1016/S2213-8587(22)00009-2.

[4] S. Patel, S. Srivastava, M.R. Singh, D. Singh, Mechanistic insight into diabetic wounds: pathogenesis, molecular targets and treatment strategies to pace wound healing, Biomed. Pharmacother. 112 (2019), 108615, https://doi.org/10.1016/j.biopha.2019.108615.

[5] M. Edmonds, C. Manu, P. Vas, The current burden of diabetic foot disease, J. Clin. Orthop. Trauma. 17 (2021) 88–93, https://doi.org/10.1016/j.jcot.2021.01.017.

[6] S.L. Wong, M. Demers, K. Martinod, M. Gallant, Y. Wang, A.B. Goldfine, C. R. Kahn, D.D. Wagner, Diabetes primes neutrophils to undergo NETosis, which impairs wound healing, Nat. Med. 21 (2015) 815–819, https://doi.org/10.1038/nm.3887.

[7] R.G. Frykberg, J. Banks, Challenges in the treatment of chronic wounds, Adv. Wound Care 4 (2015) 560–582, https://doi.org/10.1089/wound.2015.0635.

[8] S.-C. Guo, S.-C. Tao, W.-J. Yin, X. Qi, T. Yuan, C.-Q. Zhang, Exosomes derived from platelet-rich plasma promote the re-epithelization of chronic cutaneous wounds via activation of YAP in a diabetic rat model, Theranostics 7 (2017) 81–96, https://doi.org/10.7150/thno.16803.

[9] W. Chengwei, L. Yihao, Y. Xiaoxiao, L. Wentao, Z. Xianhao, R. Ya, Z. Changru, Y. Han, K. Weiqing, W. Jinwu, N. Haoyi, In-situ forming hydrogel incorporated with reactive oxygen species responsive and antibacterial properties for diabetic infected chronic wound healing, Chem. Eng. J. 450 (2022), 138077, https://doi.org/10.1016/j.cej.2022.138077.

[10] K. Glover, A.C. Stratakos, A. Varadi, D.A. Lamprou, 3D scaffolds in the treatment of diabetic foot ulcers: new trends vs conventional approaches, Int. J. Pharm. 599 (2021), 120423, https://doi.org/10.1016/j.ijpharm.2021.120423.

[11] B. Qian, Q. Yang, M. Wang, S. Huang, C. Jiang, H. Shi, Q. Long, M. Zhou, Q. Zhao, X. Ye, Encapsulation of lyophilized platelet-rich fibrin in alginate-hyaluronic acid hydrogel as a novel vascularized substitution for myocardial infarction, Bioact. Mater. 7 (2022) 401–411, https://doi.org/10.1016/j.bioactmat.2021.05.042.

[12] Y. Li, P. Song, J. He, B. Liu, S. Liu, Y. Zhou, J. Wang, Comparison between injectable platelet-rich fibrin and platelet-rich plasma in ameliorating UVA-induced photoaging in human dermal fibroblasts via the activation of TGF-β/smad signaling pathway, Photochem. Photobiol. (2022), https://doi.org/10.1111/php.13628.

[13] K.G.B. Abegão, B.N. Bracale, I.G. Delfim, E.S. dos Santos, C.B. Laposy, G.A. Nai, R. Giuffrida, R.M.B. Nogueira, Effects of heterologous platelet-rich plasma gel on standardized dermal wound healing in rabbits, Acta Cir. Bras. 30 (2015) 209–215, https://doi.org/10.1590/S0102-865020150030000008.

[14] R.C. da F. Pereira, F.D. De La Côrte, K.E. Brass, M. da Silva Azevedo, M. Gallio, C. Cantarelli, S.L. Dau, A.S. Cezar, M.A. Inkelmann, Evaluation of three methods of platelet-rich plasma for treatment of equine distal limb skin wounds, J. Equine Vet. Sci. 72 (2019) 1–7, https://doi.org/10.1016/j.jevs.2017.10.009.

[15] L.C. Garbin, C.S. Olver, Platelet-rich products and their application to osteoarthritis, J. Equine Vet. Sci. 86 (2020), 102820, https://doi.org/10.1016/j.jevs.2019.102820.

[16] C. Bottegoni, L. Dei Giudici, S. Salvemini, E. Chiurazzi, R. Bencivenga, A. Gigante, Homologous platelet-rich plasma for the treatment of knee osteoarthritis in selected elderly patients: an open-label, uncontrolled, pilot study, Ther Adv Musculoskelet Dis 8 (2016) 35–41, https://doi.org/10.1177/1759720X16631188.

[17] S. Akbarzadeh, M.B. McKenzie, M.M. Rahman, H. Cleland, Allogeneic platelet-rich plasma: is it safe and effective for wound repair? Eur. Surg. Res. 62 (2021) 1–9, https://doi.org/10.1159/000514223.

[18] P.A. Everts, G.A. Malanga, R.V. Paul, J.B. Rothenberg, N. Stephens, K.R. Mautner, Assessing clinical implications and perspectives of the pathophysiological effects of erythrocytes and plasma free hemoglobin in autologous biologics for use in musculoskeletal regenerative medicine therapies, A review, Regen. Ther. 11 (2019) 56–64, https://doi.org/10.1016/j.reth.2019.03.009.

[19] D. Li, N. Wu, Mechanism and application of exosomes in the wound healing process in diabetes mellitus, Diabetes Res. Clin. Pract. 187 (2022), 109882, https://doi.org/10.1016/j.diabres.2022.109882.

[20] A.A.Q. Ahmed, F. Qi, R. Zheng, L. Xiao, A.M.E. Abdalla, L. Mao, B.M. Bakadia, L. Liu, O.M. Atta, X. Li, Z. Shi, G. Yang, The impact of ExHp-CD (outer membrane vesicles) released from Helicobacter pylori SS1 on macrophage RAW 264.7 cells and their immunogenic potential, Life Sci. 279 (2021), 119644, https://doi.org/10.1016/j.lfs.2021.119644.

[21] S.W. Ferguson, J. Nguyen, Exosomes as therapeutics: the implications of molecular composition and exosomal heterogeneity, J. Contr. Release 228 (2016) 179–190, https://doi.org/10.1016/j.jconrel.2016.02.037.

[22] X. Wang, Y. Jiao, Y. Pan, L. Zhang, H. Gong, Y. Qi, M. Wang, H. Gong, M. Shao, X. Wang, D. Jiang, Fetal dermal mesenchymal stem cell-derived exosomes accelerate cutaneous wound healing by activating notch signaling, Stem Cell. Int. 2019 (2019) 1–11, https://doi.org/10.1155/2019/2402916.

[23] B. Hersant, M. Sid-Ahmed, L. Braud, M. Jourdan, Y. Baba-Amer, J.-P. Meningaud, A.-M. Rodriguez, Platelet-rich plasma improves the wound healing potential of mesenchymal stem cells through paracrine and metabolism alterations, Stem Cell. Int. 2019 (2019) 1–14, https://doi.org/10.1155/2019/1234263.

[24] K. Lu, K. Li, M. Zhang, Z. Fang, P. Wu, L. Feng, K. Deng, C. Yu, Y. Deng, Y. Xiao, P. Zhu, R. Guo, Adipose-derived stem cells (ADSCs) and platelet-rich plasma (PRP) loaded gelatin/silk fibroin hydrogels for improving healing in a murine pressure ulcer model, Chem. Eng. J. 424 (2021), 130429, https://doi.org/10.1016/j.cej.2021.130429.

[25] S. Bhat, P. Viswanathan, S. Chandanala, S.J. Prasanna, R.N. Seetharam, Expansion and characterization of bone marrow derived human mesenchymal stromal cells in serum-free conditions, Sci. Rep. 11 (2021) 3403, https://doi.org/10.1038/s41598-021-83088-1.

[26] B. Lopes, P. Sousa, R. Alvites, M. Branquinho, A. Sousa, C. Mendonça, L. M. Atayde, A.C. Maurício, The application of mesenchymal stem cells on wound repair and regeneration, Appl. Sci. 11 (2021) 3000, https://doi.org/10.3390/app11073000.
[27] M. Song, J. Heo, J.-Y. Chun, H.S. Bae, J.W. Kang, H. Kang, Y.M. Cho, S.W. Kim, D.-M. Shin, M.-S. Choo, The paracrine effects of mesenchymal stem cells stimulate the regeneration capacity of endogenous stem cells in the repair of a bladder-outlet-obstruction-induced overactive bladder, Stem Cell. Dev. 23 (2014) 654–663, https://doi.org/10.1089/scd.2013.0277.
[28] X. Liang, Y. Ding, Y. Zhang, H.-F. Tse, Q. Lian, Paracrine mechanisms of mesenchymal stem cell-based therapy: current status and perspectives, Cell Transplant. 23 (2014) 1045–1059, https://doi.org/10.3727/096368913X667709.
[29] R. Censi, C. Casadidio, S. Deng, M.R. Gigliobianco, M.G. Sabbieti, D. Agas, F. Laus, P. Di Martino, Interpenetrating hydrogel networks enhance mechanical stability, rheological properties, release behavior and adhesiveness of platelet-rich plasma, Int. J. Mol. Sci. 21 (2020) 1399, https://doi.org/10.3390/ijms21041399.
[30] X. Zhang, D. Yao, W. Zhao, R. Zhang, B. Yu, G. Ma, Y. Li, D. Hao, F. Xu, Engineering platelet-rich plasma based dual-network hydrogel as a bioactive wound dressing with potential clinical translational value, Adv. Funct. Mater. 31 (2021), 2009258, https://doi.org/10.1002/adfm.202009258.
[31] M. Wang, C. Wang, M. Chen, Y. Xi, W. Cheng, C. Mao, T. Xu, X. Zhang, C. Lin, W. Gao, Y. Guo, B. Lei, Efficient angiogenesis-based diabetic wound healing/skin reconstruction through bioactive antibacterial adhesive ultraviolet shielding nanodressing with exosome release, ACS Nano 13 (2019) 10279–10293, https://doi.org/10.1021/acsnano.9b03656.
[32] S.S. Rao, A. Prabhu, J. Kudkuli, S. Surya, P.D. Rekha, Hyaluronic acid sustains platelet stability with prolonged growth factor release and accelerates wound healing by enhancing proliferation and collagen deposition in diabetic mice, J. Drug Deliv. Sci. 67 (2022), 102898, https://doi.org/10.1016/j.jddst.2021.102898.
[33] C. Wang, M. Wang, T. Xu, X. Zhang, C. Lin, W. Gao, H. Xu, B. Lei, C. Mao, Engineering bioactive self-healing antibacterial exosomes hydrogel for promoting chronic diabetic wound healing and complete skin regeneration, Theranostics 9 (2019) 65–76, https://doi.org/10.7150/thno.29766.
[34] W. Chu, M. Nie, X. Ke, J. Luo, J. Li, Recent advances in injectable dual crosslinking hydrogels for biomedical applications, Macromol. Biosci. 21 (2021), 2100109, https://doi.org/10.1002/mabi.202100109.
[35] G. Das, H.-S. Shin, E.V.R. Campos, L.F. Fraceto, M. del Pilar Rodriguez-Torres, K. C.F. Mariano, D.R. de Araujo, F. Fernández-Luqueño, R. Grillo, J.K. Patra, Sericin based nanoformulations: a comprehensive review on molecular mechanisms of interaction with organisms to biological applications, J. Nanobiotechnol. 19 (2021) 30, https://doi.org/10.1186/s12951-021-00774-y.
[36] B.M. Bakadia, A. Zhong, X. Li, B.O.O. Boni, A.A.Q. Ahmed, T. Souho, R. Zheng, Z. Shi, D. Shi, L. Lamboni, G. Yang, Biodegradable and injectable poly(vinyl alcohol) microspheres in silk sericin-based hydrogel for the controlled release of antimicrobials: application to deep full-thickness burn wound healing, Adv. Compos. Hybrid Mater. (2022), https://doi.org/10.1007/s42114-022-00467-6.
[37] B.M. Bakadia, L. Lamboni, A.A. Qaed Ahmed, R. Zheng, B.O. Ode Boni, Z. Shi, S. Song, T. Souho, B.M. Mukole, F. Qi, G. Yang, Antibacterial silk sericin/poly (vinyl alcohol) hydrogel with antifungal property for potential infected large burn wound healing: systemic evaluation, Smart Mater. Med. 4 (2023) 37–58, https://doi.org/10.1016/j.smaim.2022.07.002.
[38] C. Lujerdean, G.-M. Baci, A.-A. Cucu, D.S. Dezmirean, The contribution of silk fibroin in biomedical engineering, Insects 13 (2022), https://doi.org/10.3390/insects13030286.
[39] S. Lv, Silk fibroin-based materials for catalyst immobilization, Molecules 25 (2020), https://doi.org/10.3390/molecules25214929.
[40] Y.R. Park, M.T. Sultan, H.J. Park, J.M. Lee, H.W. Ju, O.J. Lee, D.J. Lee, D. L. Kaplan, C.H. Park, NF-κB signaling is key in the wound healing processes of silk fibroin, Acta Biomater. 67 (2018) 183–195, https://doi.org/10.1016/j.actbio.2017.12.006.
[41] J. Liu, L. Shi, Y. Deng, M. Zou, B. Cai, Y. Song, Z. Wang, L. Wang, Silk sericin-based materials for biomedical applications, Biomaterials 287 (2022), 121638, https://doi.org/10.1016/j.biomaterials.2022.121638.
[42] A. Bucciarelli, A. Motta, Use of Bombyx mori silk fibroin in tissue engineering: from cocoons to medical devices, challenges, and future perspectives, Biomater. Adv. 139 (2022), 212982, https://doi.org/10.1016/j.bioadv.2022.212982.
[43] W. Zhang, L. Chen, J. Chen, L. Wang, X. Gui, J. Ran, G. Xu, H. Zhao, M. Zeng, J. Ji, L. Qian, J. Zhou, H. Ouyang, X. Zou, Silk fibroin biomaterial shows safe and effective wound healing in animal models and a randomized controlled clinical trial, Adv. Healthc. Mater. 6 (2017), 1700121, https://doi.org/10.1002/adhm.201700121.
[44] J.W. Weisel, R.I. Litvinov, Fibrin Formation, structure and properties, Subcell. Biochem. 82 (2017) 405–456, https://doi.org/10.1007/978-3-319-49674-0_13.
[45] W.-Q. Chen, H. Priewalder, J.P. Pradeep John, G. Lubec, Silk cocoon of Bombyx mori : proteins and posttranslational modifications - heavy phosphorylation and evidence for lysine-mediated cross links, Proteomics 10 (2010) 369–379, https://doi.org/10.1002/pmic.200900624.
[46] K.M. Babu, Silk fibres, in: Handb. Nat. Fibres, Elsevier, 2012, pp. 146–170, https://doi.org/10.1533/9780857095503.1.146.
[47] K. Murugesh Babu, Structural aspects of silk, in: Silk, Elsevier, 2013, pp. 56–83, https://doi.org/10.1533/9781782421580.56.
[48] R.I. Kunz, R.M.C. Brancalhão, L. de F.C. Ribeiro, M.R.M. Natali, Silkworm sericin: properties and biomedical applications, BioMed Res. Int. 2016 (2016) 1–19, https://doi.org/10.1155/2016/8175701.
[49] F. Wurm, B. Rietzler, T. Pham, T. Bechtold, Multivalent ions as reactive crosslinkers for biopolymers—a review, Molecules 25 (2020) 1840, https://doi.org/10.3390/molecules25081840.
[50] Y. Zhao, Z.S. Zhu, J. Guan, S.J. Wu, Processing, mechanical properties and bio-applications of silk fibroin-based high-strength hydrogels, Acta Biomater. 125 (2021) 57–71, https://doi.org/10.1016/j.actbio.2021.02.018.
[51] C. Théry, S. Amigorena, G. Raposo, A. Clayton, Isolation and characterization of exosomes from cell culture supernatants and biological fluids, Curr. Protoc. Cell Biol. Chapter 3 (2006), https://doi.org/10.1002/0471143030.cb0322s30. Unit 3.22.
[52] R.M. Zaremba, A.C. Brooks, E.J. Thomovsky, G.E. Moore, P.A. Johnson, Comparison of a commercial immunochromatographic strip crossmatch kit and standard laboratory crossmatch methods for blood transfusion compatibility in dogs, J. Vet. Emerg. Crit. Care (2022), https://doi.org/10.1111/vec.13219.
[53] P. Jayakumar, S. Padmanabhan, K. Suthendran, G.V. Rajveer, Development of safe semi-automatic and economic blood cross matching using image processing, Mater. Today: Proc. 44 (2021) 3536–3539, https://doi.org/10.1016/j.matpr.2020.09.293.
[54] K. Rattanasuwan, S. Rassameemasmaung, S. Kiattavorncharoen, A. Sirikulsathean, J. Thorsuwan, W. Wongsankakorn, Platelet-rich plasma stimulated proliferation, migration, and attachment of cultured periodontal ligament cells., Eur. J. Dermatol. 12 (n.d.) 469–474. https://doi.org/10.4103/ejd.ejd_255_17.
[55] A.F. Grecu, D.C. Grecu, O. Nica, E.M. Ciuca, A. Camen, M.E. Ciurea, A novel method of obtaining platelet rich fibrin from rats and quantifying platelet count, Curr. Heal. Sci. J. 45 (2019) 104–110, https://doi.org/10.12865/CHSJ.45.01.14.
[56] A. Di Martino, A. Boffa, L. Andriolo, I. Romandini, S.A. Altamura, A. Cenacchi, V. Roverini, S. Zaffagnini, G. Filardo, Leukocyte-rich versus leukocyte-poor platelet-rich plasma for the treatment of knee osteoarthritis: a double-blind randomized trial, Am. J. Sports Med. 50 (2022) 609–617, https://doi.org/10.1177/03635465211064303.
[57] E. Anitua, M. Zalduendo, M. Troya, S. Padilla, G. Orive, Leukocyte inclusion within a platelet rich plasma-derived fibrin scaffold stimulates a more pro-inflammatory environment and alters fibrin properties, PLoS One 10 (2015), e0121713, https://doi.org/10.1371/journal.pone.0121713.
[58] K. Segawa, T. Kondo, S. Kimura, A. Fujimoto, T. Kato, T. Ishikawa, S. Neo, M. Hisasue, T. Yamada, R. Tsuchiya, Effects of prostaglandin E1 on the preparation of platelet concentrates in dogs., J. Vet. Intern. Med. 26 (n.d.) 370–376. https://doi.org/10.1111/j.1939-1676.2011.00881.x.
[59] R.P. Kreutz, P. Nystrom, Y. Kreutz, J. Miao, R. Kovacs, Z. Desta, D.A. Flockhart, Y. Jin, Inhibition of platelet aggregation by prostaglandin E1 (PGE1) in diabetic patients during therapy with clopidogrel and aspirin, Platelets 24 (2013) 145–150, https://doi.org/10.3109/09537104.2012.661107.
[60] C. Cavallo, A. Roffi, B. Grigolo, E. Mariani, L. Pratelli, G. Merli, E. Kon, M. Marcacci, G. Filardo, Platelet-rich plasma: the choice of activation method affects the release of bioactive molecules, BioMed Res. Int. (2016), https://doi.org/10.1155/2016/6591717 n.d.) 6591717.
[61] S.R. Iyer, A.L. Scheiber, P. Yarowsky, R.F. Henn, S. Otsuru, R.M. Lovering, Exosomes isolated from platelet-rich plasma and mesenchymal stem cells promote recovery of function after muscle injury, Am. J. Sports Med. 48 (2020) 2277–2286, https://doi.org/10.1177/0363546520926462.
[62] C. Leiva-Sabadini, S. Alvarez, N.P. Barrera, C.M. Schuh, S. Aguayo, Antibacterial effect of honey-derived exosomes containing antimicrobial peptides against oral streptococci, Int. J. Nanomed. 16 (2021) 4891–4900, https://doi.org/10.2147/IJN.S315040.
[63] B.M. Bakadia, B.O.O. Boni, A.A.Q. Ahmed, R. Zheng, Z. Shi, M.W. Ullah, L. Lamboni, G. Yang, In situ synthesized porous bacterial cellulose/poly(vinyl alcohol)-based silk sericin and azithromycin release system for treating chronic wound biofilm, Macromol. Biosci. (2022), 2200201, https://doi.org/10.1002/mabi.202200201.
[64] Zainuddin, D.J.T. Hill, A.K. Whittaker, L. Lambert, T.V. Chirila, Preferential interactions of calcium ions in poly(2-hydroxyethyl methacrylate) hydrogels, J. Mater. Sci. Mater. Med. 18 (2007) 1141–1149, https://doi.org/10.1007/s10856-007-0135-0.
[65] R.H. Ellerbrock, H.H. Gerke, FTIR spectral band shifts explained by OM–cation interactions, J. Plant Nutr. Soil Sci. 184 (2021) 388–397, https://doi.org/10.1002/jpln.202100056.
[66] P. Xu, J. Song, Z. Dai, Y. Xu, D. Li, C. Wu, Effect of Ca2+ cross-linking on the properties and structure of lutein-loaded sodium alginate hydrogels, Int. J. Biol. Macromol. 193 (2021) 53–63, https://doi.org/10.1016/j.ijbiomac.2021.10.114.
[67] Y. Bao, H. Zhang, L. Chen, H.-H. Cai, Z.-L. Liu, Y. Peng, Z. Li, F.-Y. Dai, Artemisinin-loaded silk fibroin/gelatin composite hydrogel for wound healing and tumor therapy, Arab. J. Chem. 16 (2023), 104782, https://doi.org/10.1016/j.arabjc.2023.104782.
[68] E. Arjeh, H. Rostami, S. Pirsa, M. Fathi, Synthesis and characterization of novel Spirulina protein isolate (SPI)-based hydrogels through dual-crosslinking with genipin/Zn2+, Food Res. Int. 162 (2022), 112107 https://doi.org/10.1016/j.foodres.2022.112107.
[69] S. Teimouri, C. Dekiwadia, S. Kasapis, Decoupling diffusion and macromolecular relaxation in the release of vitamin B6 from genipin-crosslinked whey protein networks, Food Chem. 346 (2021), 128886, https://doi.org/10.1016/j.foodchem.2020.128886.

[70] W.-C. Ng, Y. Lokanathan, M.B. Fauzi, M.M. Baki, A.A. Zainuddin, S.J. Phang, M. Azman, In vitro evaluation of genipin-crosslinked gelatin hydrogels for vocal fold injection, Sci. Rep. 13 (2023) 5128, https://doi.org/10.1038/s41598-023-32080-y.
[71] T. Imsombut, Y. Srisuwan, P. Srihanam, Y. Baimark, Genipin-cross-linked silk fibroin microspheres prepared by the simple water-in-oil emulsion solvent diffusion method, Powder Technol. 203 (2010) 603–608, https://doi.org/10.1016/j.powtec.2010.06.027.
[72] B. Qian, Q. Yang, M. Wang, S. Huang, C. Jiang, H. Shi, Q. Long, M. Zhou, Q. Zhao, X. Ye, Encapsulation of lyophilized platelet-rich fibrin in alginate-hyaluronic acid hydrogel as a novel vascularized substitution for myocardial infarction, Bioact. Mater. 7 (2022) 401–411, https://doi.org/10.1016/j.bioactmat.2021.05.042.
[73] X. Liu, L. Wang, C. Ma, G. Wang, Y. Zhang, S. Sun, Exosomes derived from platelet-rich plasma present a novel potential in alleviating knee osteoarthritis by promoting proliferation and inhibiting apoptosis of chondrocyte via Wnt/β-catenin signaling pathway, J. Orthop. Surg. Res. 14 (2019) 470, https://doi.org/10.1186/s13018-019-1529-7.
[74] E. Mariani, A. Roffi, L. Cattini, L. Pulsatelli, E. Assirelli, G.S. Krishnakumar, A. Cenacchi, E. Kon, G. Filardo, Release kinetic of pro- and anti-inflammatory biomolecules from platelet-rich plasma and functional study on osteoarthritis synovial fibroblasts, Cytotherapy 22 (2020) 344–353, https://doi.org/10.1016/j.jcyt.2020.02.006.
[75] K. Wang, J. Li, Y. Wang, Y. Wang, Y. Qin, F. Yang, M. Zhang, H. Zhu, Z. Li, Orchestrated cellular, biochemical, and biomechanical optimizations endow platelet-rich plasma-based engineered cartilage with structural and biomechanical recovery, Bioact. Mater. 6 (2021) 3824–3838, https://doi.org/10.1016/j.bioactmat.2021.03.037.
[76] F. Sadeghpour Heravi, M. Zakrzewski, K. Vickery, D.G. Armstrong, H. Hu, Bacterial diversity of diabetic foot ulcers: current status and future prospectives, J. Clin. Med. 8 (2019), https://doi.org/10.3390/jcm8111935.
[77] J.L. Lázaro Martínez, Y. García Álvarez, A. Tardáguila-García, E. García Morales, Optimal management of diabetic foot osteomyelitis: challenges and solutions, Diabetes, Metab. Syndrome Obes. Targets Ther. 12 (2019) 947–959, https://doi.org/10.2147/DMSO.S181198.
[78] L. Giurato, M. Meloni, V. Izzo, L. Uccioli, Osteomyelitis in diabetic foot: a comprehensive overview, World J. Diabetes 8 (2017) 135, https://doi.org/10.4239/wjd.v8.i4.135.
[79] E.A. Masters, R.P. Trombetta, K.L. de Mesy Bentley, B.F. Boyce, A.L. Gill, S.R. Gill, K. Nishitani, M. Ishikawa, Y. Morita, H. Ito, S.N. Bello-Irizarry, M. Ninomiya, J. D. Brodell, C.C. Lee, S.P. Hao, I. Oh, C. Xie, H.A. Awad, J.L. Daiss, J.R. Owen, S. L. Kates, E.M. Schwarz, G. Muthukrishnan, Evolving concepts in bone infection: redefining “biofilm”, “acute vs. chronic osteomyelitis”, “the immune proteome” and “local antibiotic therapy,” Bone Res 7 (2019) 20, https://doi.org/10.1038/s41413-019-0061-z.
[80] B.M. Bakadia, F. He, T. Souho, L. Lamboni, M.W. Ullah, B.O. Boni, A.A.Q. Ahmed, B.M. Mukole, G. Yang, Prevention and treatment of COVID-19: focus on interferons, chloroquine/hydroxychloroquine, azithromycin, and vaccine, Biomed. Pharmacother. 133 (2021), 111008, https://doi.org/10.1016/j.biopha.2020.111008.
[81] A. Cieślik-Bielecka, T. Bold, G. Ziółkowski, M. Pierchała, A. Królikowska, P. Reichert, Antibacterial activity of leukocyte- and platelet-rich plasma: an in vitro study, BioMed Res. Int. 2018 (2018) 1–8, https://doi.org/10.1155/2018/9471723.
[82] V. Viswanathan, S. Pendsey, C. Radhakrishnan, T.D. Rege, J. Ahdal, R. Jain, Methicillin-resistant Staphylococcus aureus in diabetic foot infection in India: a growing menace, Int. J. Low. Extrem. Wounds 18 (2019) 236–246, https://doi.org/10.1177/1534734619853668.
[83] W. Chai, Y. Wang, H. Zheng, S. Yue, Y. Liu, Y. Wu, X. Li, The profile of microbiological pathogens in diabetic foot ulcers, Front. Med. 8 (2021), https://doi.org/10.3389/fmed.2021.656467.
[84] A. Cieslik-Bielecka, D.M. Dohan Ehrenfest, A. Lubkowska, T. Bielecki, Microbicidal properties of leukocyte- and platelet-rich plasma/fibrin (L-PRP/L-PRF): new perspectives, J. Biol. Regul. Homeost. Agents 26 (2012) 43S–52S. http://www.ncbi.nlm.nih.gov/pubmed/23648198.
[85] H.A. Farghali, N.A. AbdElKader, H.O. AbuBakr, S.H. Aljuaydi, M.S. Khattab, R. Elhelw, M. Elhariri, Antimicrobial action of autologous platelet-rich plasma on MRSA-infected skin wounds in dogs, Sci. Rep. 9 (2019), 12722, https://doi.org/10.1038/s41598-019-48657-5.
[86] A.A.Q. Ahmed, R. Zheng, A.M.E. Abdalla, B.M. Bakadia, F. Qi, L. Xiao, O.M. Atta, L. Mao, G. Yang, Heterogeneous populations of outer membrane vesicles released from Helicobacter pylori SS1 with distinct biological properties, Eng. Sci. 15 (2021) 148–165, https://doi.org/10.30919/es8d470.
[87] P. Krzyszczyk, R. Schloss, A. Palmer, F. Berthiaume, The role of macrophages in acute and chronic wound healing and interventions to promote pro-wound healing phenotypes, Front. Physiol. 9 (2018) 419, https://doi.org/10.3389/fphys.2018.00419.
[88] C. Yunna, H. Mengru, W. Lei, C. Weidong, Macrophage M1/M2 polarization, Eur. J. Pharmacol. 877 (2020), 173090, https://doi.org/10.1016/j.ejphar.2020.173090.
[89] X. Wu, W. He, X. Mu, Y. Liu, J. Deng, Y. Liu, X. Nie, Macrophage polarization in diabetic wound healing, Burn. Trauma. 10 (2022), https://doi.org/10.1093/burnst/tkac051 tkac051.
[90] A.C. Trombetta, S. Soldano, P. Contini, V. Tomatis, B. Ruaro, S. Paolino, R. Brizzolara, P. Montagna, A. Sulli, C. Pizzorni, V. Smith, M. Cutolo, A circulating cell population showing both M1 and M2 monocyte/macrophage surface markers characterizes systemic sclerosis patients with lung involvement, Respir. Res. 19 (2018) 186, https://doi.org/10.1186/s12931-018-0891-z.
[91] J. Dai, J. Shen, Y. Chai, H. Chen, IL-1β impaired diabetic wound healing by regulating MMP-2 and MMP-9 through the p38 pathway, Mediat. Inflamm. 2021 (2021) 1–10, https://doi.org/10.1155/2021/6645766.
[92] S.-M. Huang, C.-S. Wu, M.-H. Chiu, C.-H. Wu, Y.-T. Chang, G.-S. Chen, C.-C. E. Lan, High glucose environment induces M1 macrophage polarization that impairs keratinocyte migration via TNF-α: an important mechanism to delay the diabetic wound healing, J. Dermatol. Sci. 96 (2019) 159–167, https://doi.org/10.1016/j.jdermsci.2019.11.004.
[93] M. Misiura, T. Guszczyn, I. Oscilowska, W. Baszanowska, J. Palka, W. Miltyk, Platelet-rich plasma promotes the proliferation of human keratinocytes via a progression of the cell cycle. A role of prolidase, Int. J. Mol. Sci. 22 (2021), https://doi.org/10.3390/ijms22020936.
[94] K.E. Johnson, T.A. Wilgus, Vascular endothelial growth factor and angiogenesis in the regulation of cutaneous wound repair, Adv. Wound Care 3 (2014) 647–661, https://doi.org/10.1089/wound.2013.0517.
[95] P. Kolimi, S. Narala, D. Nyavanandi, A.A.A. Youssef, N. Dudhipala, Innovative treatment strategies to accelerate wound healing: trajectory and recent advancements, Cells 11 (2022) 2439, https://doi.org/10.3390/cells11152439.
[96] M. Kandhwal, T. Behl, S. Singh, N. Sharma, S. Arora, S. Bhatia, A. Al-Harrasi, M. Sachdeva, S. Bungau, Role of matrix metalloproteinase in wound healing, Am. J. Transl. Res. 14 (2022) 4391–4405. http://www.ncbi.nlm.nih.gov/pubmed/35958464.
[97] D.J. Gibson, G.S. Schultz, Molecular wound assessments: matrix metalloproteinases, Adv. Wound Care 2 (2013) 18–23, https://doi.org/10.1089/wound.2011.0359.
[98] T. Tokuhiro, A. Ishikawa, H. Sato, S. Takita, A. Yoshikawa, R. Anzai, S. Sato, R. Aoyagi, M. Arita, T. Shibuya, Y. Aratani, S. Shimizu, M. Tanaka, S. Yotsumoto, Oxidized phospholipids and neutrophil elastase coordinately play critical roles in NET formation, Front. Cell Dev. Biol. 9 (2021), https://doi.org/10.3389/fcell.2021.718586.
[99] S. Yang, Z. Gu, C. Lu, T. Zhang, X. Guo, G. Xue, L. Zhang, Neutrophil extracellular traps are markers of wound healing impairment in patients with diabetic foot ulcers treated in a multidisciplinary setting, Adv. Wound Care 9 (2020) 16–27, https://doi.org/10.1089/wound.2019.0943.
[100] H. Parker, C.C. Winterbourn, Reactive oxidants and myeloperoxidase and their involvement in neutrophil extracellular traps, Front. Immunol. 3 (2013), https://doi.org/10.3389/fimmu.2012.00424.
[101] T.G. Sahana, P.D. Rekha, Biopolymers: applications in wound healing and skin tissue engineering, Mol. Biol. Rep. 45 (2018) 2857–2867, https://doi.org/10.1007/s11033-018-4296-3.
[102] H. Aldehlawi, S. Usman, A. Lalli, F. Ahmad, G. Williams, M.-T. Teh, A. Waseem, Serum lipids, retinoic acid and phenol red differentially regulate expression of keratins K1, K10 and K2 in cultured keratinocytes, Sci. Rep. 10 (2020) 4829, https://doi.org/10.1038/s41598-020-61640-9.